

Review

A Review on the Progress and Future of TiO₂/Graphene Photocatalysts

Amara Nasir ^{1,2}, Sadia Khalid ³, Tariq Yasin ² and Anca Mazare ^{4,5,*}

¹ Department of Physics & Applied Mathematics, Pakistan Institute of Engineering and Applied Sciences (PIEAS), PO Nilore, Islamabad 45650, Pakistan

² Department of Chemistry, Pakistan Institute of Engineering and Applied Sciences (PIEAS), PO Nilore, Islamabad 45650, Pakistan

³ Nanoscience & Technology Department, National Centre for Physics, Quaid-i-Azam University Campus, Islamabad 45320, Pakistan

⁴ Department of Materials Science WW4-LKO, Friedrich Alexander University of Erlangen Nürnberg, Martensstrasse 7, 91058 Erlangen, Germany

⁵ Advanced Institute for Materials Research (AIMR), National University Corporation Tohoku University, Sendai 980-8577, Japan

* Correspondence: anca.mazare@fau.de

Abstract: TiO₂ is seen as a low cost, well-known photocatalyst; nevertheless, its sluggish charge kinetics does limit its applications. To overcome this aspect, one of the recent approaches is the use of its composites with graphene to enhance its photoactivity. Graphene-based materials (nanosheets, quantum dots, etc.) allow for attachment with TiO₂ nanostructures, resulting in synergistic properties and thus increasing the functionality of the resulting composite. The current review aims to present the marked progress recently achieved in the use of TiO₂/graphene composites in the field of photocatalysis. In this respect, we highlight the progress and insights in TiO₂ and graphene composites in photocatalysis, including the basic mechanism of photocatalysis, the possible design strategies of the composites and an overview of how to characterize the graphene in the mixed composites. The use of composites in photocatalysis has also been reviewed, in which the recent literature has opened up more questions related to the reliability, potential, repeatability and connection of photocatalytic mechanisms with the resulting composites. TiO₂/graphene-based composites can be a green light in the future of photocatalysis, targeting pollution remediation, energy generation, etc.

Keywords: titanium dioxide; graphene; nanomaterials; photocatalysis



Citation: Nasir, A.; Khalid, S.; Yasin, T.; Mazare, A. A Review on the Progress and Future of TiO₂/Graphene Photocatalysts. *Energies* **2022**, *15*, 6248. <https://doi.org/10.3390/en15176248>

Academic Editors: Lifang Chen, Luis Enrique Noreña and Jin An Wang

Received: 31 July 2022

Accepted: 23 August 2022

Published: 27 August 2022

Publisher's Note: MDPI stays neutral with regard to jurisdictional claims in published maps and institutional affiliations.



Copyright: © 2022 by the authors. Licensee MDPI, Basel, Switzerland. This article is an open access article distributed under the terms and conditions of the Creative Commons Attribution (CC BY) license (<https://creativecommons.org/licenses/by/4.0/>).

1. Introduction

Photocatalysis involves the direct use of perpetual sunlight as an energy source and therefore has become a spotlight of mainstream researchers. TiO₂ is a promising semiconductor photocatalyst due to its low toxicity, low cost, stability and a favorable bandgap and band edge position for photocatalytic applications. The search for a composite photocatalyst of TiO₂ arises from the limitations of using TiO₂, which include low absorption in the visible range of the solar spectrum, sluggish charge transfer kinetics and, primarily, the inevitable precious metal consumption for obtaining satisfactory performance in practical applications [1,2]. Overcoming the limitations present in photocatalysis over TiO₂, as well as the search for metal-free photocatalysts for the modification of TiO₂ with carbon-based materials, in particular with graphene, has been a focus of current research [1,3,4]. Recently, abundant research towards TiO₂/graphene-based photocatalysts has been witnessed, as evidenced by the increasing number of publications reported in the last three years (2022—12,300, 2021—15,200, 2020—11,900, source: Google scholar, keyword: TiO₂/graphene photocatalyst).

Graphene is an exceptional material with a two-dimensional carbon sheet structure that presents very unique electrical, electronic, optical, thermal and surface features. Combined with a semiconductor, it can serve as a good electron sink or a support to separate and

transport the charge effectively in photocatalytic reactions [3,4]. The key lies in its favorable bandgap and unique electrical and electronic properties, which make it a potential macromolecular: (i) photocatalyst, (ii) photosensitizer under visible illumination or (iii) cocatalyst in a composite photocatalyst [5,6]. Its unique surface can also provide copious active sites for redox reactions and to chemisorb molecules [7,8]. Its polar derivative, graphene oxide (GO) or reduced graphene oxide (RGO), has been reported to form unique mixed composites with polymers [9] and semiconductors [10] in view of in-demand applications, including, for instance, water remediation, energy storage devices, photocatalysis, etc. [11]. They possess a variety of oxygen functional groups (carboxyl, hydroxyl, carbonyl and epoxy) which can form chemical bonds with TiO_2 , and this results in composites with compatible interfaces and synergistic features [12].

Herein, we have highlighted the critical aspects and key features in TiO_2 /graphene photocatalysts, considering also the recent marked interest in this field. We have first included a brief overview of the basics involved in photocatalysis over TiO_2 , followed by a discussion of the crucial factors affecting the use of TiO_2 or graphene oxide as a photocatalyst, including the role of graphene in a photocatalytic system. The progress in obtaining and characterizing these composites together with their use in photocatalysis has also been overviewed, resulting in a “how to” guide. This review provides a one-click overview of TiO_2 /graphene photocatalysts, including current status, insights, progress, limitations to be addressed and future use.

2. Photocatalysis Over TiO_2 : The Basics

TiO_2 is one of the most used semiconductor photocatalysts due to its nontoxicity, stability in aqueous solutions, good quantum efficiencies and suitable bandgap [13]. Under illumination, electrons are promoted to the conduction band (CB) of TiO_2 from the valence band (VB), thereby leaving an electron vacancy, or the hole in the VB, as seen in Figure 1. However, this happens only if the energy of the photon is equal to or greater than the bandgap energy of the photocatalyst, i.e., in our case, TiO_2 [14]. Moreover, for TiO_2 photocatalysts, UV light illumination results in photoexcitation as a result of the bandgap energy of the TiO_2 photocatalyst, which, for anatase is 3.2 eV ($\lambda = 385$ nm) and for rutile is 3.0 eV ($\lambda = 410$ nm) [15].

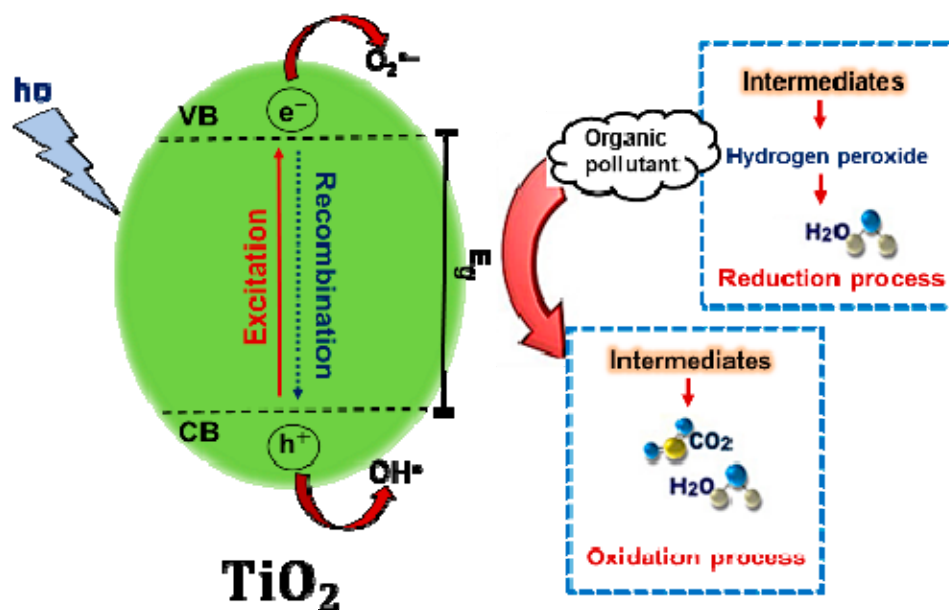


Figure 1. Schematic illustration of typical photocatalysis over TiO_2 .

Photoexcitation results in the formation of photogenerated electron–hole pairs, and the generated charge pairs can either contribute to a chemical reaction with adsorbed/surface

species or undergoes recombination [14,16]. In a typical TiO_2 photocatalyst, the electron–hole pair can then follow the ensuing sequence of chemical reactions. Namely, the CB electron interacts with molecular oxygen and leads to the formation of a superoxide radical anion ($\text{O}_2^{\bullet-}$), and the VB hole contributes to the water/hydroxide ion oxidation and hence the formation of a hydroxyl radical (OH^\bullet) [14,16]. These generated radicals can then be further involved in different reactions as a result of photocatalysis over TiO_2 , e.g., in reactions such as nitrogen fixation [17], CO_2 reduction [18], hydrogen gas production [19], and the degradation of different pollutants [20]. In the presence of a pollutant (i.e., rhodamine B [21], congo red, methyl orange, or methylene blue dye [22]), VB holes and CB electrons can directly interact with the pollutant species and lead to pollutant mineralization due to water and dioxygen radical formation [23,24].

2.1. Mechanism of Oxidation

In a general photocatalytic reaction, the photogenerated holes oxidize water (commonly the surface of a photocatalyst contains water and is generally referred to as adsorbed water). As previously mentioned, the oxidation of water results in the formation of OH^\bullet radicals, which are, by nature, strong oxidizing agents and decompose dye [25]. In the presence of an organic dye and oxygen, there is the formation of some intermediate radicals in organic compounds [26]. This can result in radical chain reactions along with the consumption of oxygen and finally in the decomposition of organic matter into water and carbon dioxide [27–30].

2.2. Mechanism of Reduction

The reduction process in photocatalysis usually occurs in the presence of air; therefore, it can be simply seen as the reduction of oxygen. The oxygen reduction reaction occurs as an alternative to hydrogen generation reaction [29], and this is due to the fact that oxygen is a relatively easily reducible species. The $\text{O}_2^{\bullet-}$ radicals formed as a result of the interaction between the CB electrons with dissolved oxygen further react with the intermediate organic products formed during the oxidation reaction, thereby either producing peroxide or decomposing to hydrogen peroxide and then to water. Such reduction reactions are more frequent when photocatalytic processes occur in organic-compound-containing media, rather than in pure water. Therefore, the presence of organic matter on the TiO_2 surface leads to the hindrance of charge recombination and hence to promoting photocatalytic activity, and as more organic matter is present, there are more positive holes as well [27–30].

3. TiO_2 —Dependent Factors Affecting Photocatalysis

Photocatalysis is one of the most frequently used green sustainable technologies for environmental remediation [31]. Remarkable research and development has been conducted in semiconductor-photocatalysis-based applications such as solar cells, water splitting, photodynamic therapy, bacterial disinfection and, particularly, for the removal of environmental pollutants [32]. In this context, for a decade, titanium dioxide (titania or TiO_2) has remained one of the most extensively investigated semiconductor photocatalysts, owing to its suitable band gap (anatase TiO_2 —3.2 eV), chemical stability and non-toxicity [33]. TiO_2 nanophotocatalysts provide increased effective photocatalytic activity under real conditions due to their higher specific surface area compared to bulk TiO_2 [34].

The overall photocatalytic activity of TiO_2 can be influenced by the physiochemical, chemical and optoelectronic properties of the TiO_2 photocatalysts, which consequently vary depending on the synthesis method, reaction conditions (precursors, reaction medium or solvent, pH, time, reaction temperature, calcination temperature, etc.) and photocatalytic experimental conditions, such as pH, concentration, illumination power, etc. [35–37]. The key properties of TiO_2 that can be tuned by the synthesis method include the crystal phase, crystal lattice, exposed crystal facets, uncoordinated surface sites, interface, specific surface area, degree of crystallinity, geometry, size, porosity, composition, lattice defects, etc. [38–40]. From these various properties, the crystal phase,

morphology, pore size, band gap, active sites, use of sacrificial agent, dopants, cocatalysts and interfacial defects are the leading factors directing the efficiency of the TiO₂ photocatalyst's photocatalytic activity. Some of these key factors that influence the photocatalysis of TiO₂ are further discussed below.

3.1. Morphology

The morphology of the TiO₂ photocatalyst not only affects the separation of photogenerated charge carriers but also the type of the defects that originate during the synthesis. Nanostructured TiO₂ exhibits an increased number of active sites, as a result of the higher surface-to-volume ratio, and subsequently, such nanostructured photocatalysts that also have a larger specific surface area show improved photocatalytic activity and efficiency. Different TiO₂ nanostructures, such as quantum dots [41], nanoparticles [42], nanotubes [43], nanorods [44], nanosheets [45], nanoflakes [46] and hierarchically porous monoliths [47], can be prepared by sol-gel, hydrothermal/solvothermal, flame hydrolysis, water-in-oil microemulsion and chemical vapor deposition [48]. The morphology and geometry of TiO₂ nanostructures can also modify the optoelectronic properties (e.g., mid-band-gap electronic states) that can shift the absorption spectrum and alter the charge separation/migration.

Recently, Li et al. [46] investigated the impact of different TiO₂ morphologies on photocatalytic hydrogen evolution. Structure engineering via the thermal transformation of protonic titanate as a template was studied for the synthesis of TiO₂ nanoflakes (length: 100–200 nm, width: 50–100 nm), nanorods (length: 3–7 μm, width: 800–1000 nm), nanowires (length: 2–5 μm, width: 80–120 nm) and nanoflowers (diameter: 500 nm) by varying experimental conditions. The following fabrication steps were followed, as schematically represented in Figure 2: (a) nanoflakes by hydrothermal alkalization, the protonation of as-prepared titanium glycolate precursor (TGP) and calcination; (b) nanowires by hydrothermal and reflux alkalization of TGP and by calcination; (c) nanoflowers by hydrothermal alkalization and protonation and by calcination; (d) nanowires by hydrothermal alkalization, protonation and calcination of TiO₂ nanoparticles; and (e) nanoflowers by solvothermal method using tetrabutyl orthotitanate (TBT) in the presence of mixed solvents N,N-dimethylformamide (DMF) and isopropyl alcohol (IPA) and then by calcination. The highest hydrogen evolution rate of 3.63 mmol g⁻¹h⁻¹ was observed for TiO₂ nanoflakes as compared to nanorods, nanowires and nanoflowers. The exceptional photocatalytic hydrogen evolution was attributed to: (i) the negative conduction band position, (ii) fast photoinduced charge carrier separation and (iii) abundant active sites.

3.2. Phase

The three main polymorphs of TiO₂, namely, anatase, rutile and brookite, are stable under ambient and low-pressure conditions, and in addition, their relative stability varies with particle size. For example, rutile in a bulk form is thermodynamically the most stable polymorph of TiO₂, and at the nanoscale, anatase is the most stable phase. Brookite is considered a metastable form [49]. The geometric (crystallographic orientations) and electronic structure of TiO₂ influence the photocatalytic activity, i.e., anatase (indirect band gap, E_g = 3.2 eV) and rutile (direct band gap, E_g = 3.0 eV) show the maximum photoactivity among all phases. Typically, anatase is considered the most promising phase due to its higher value of reduction potential and slow recombination rate of photoexcited electrons and holes, but it also has a limited absorption in the ultraviolet (UV) region of only 4% of the solar spectrum (as a consequence of the wider band gap) [50,51].

3.3. Surface

The surface chemistry, active sites, reactive facets and interfaces are additional crucial factors that define the efficiency of the TiO₂ photocatalysts [52]. The promotion of the proton transfer between the different interfaces improves the surface chemical reactions and hence the efficiency of the photocatalyst [53]. Modification strategies for tailoring the surface properties of TiO₂ photocatalysts through doping [54], co-doping [55], defect

creation [56,57], sensitization [56], surface coatings and heterojunction formation using functional nanomaterials (oxides, plasmonic metals, quantum dots, graphene-based nanomaterials, macromolecules, etc.) [52,58,59] have been widely investigated to enhance the photocatalytic performance.

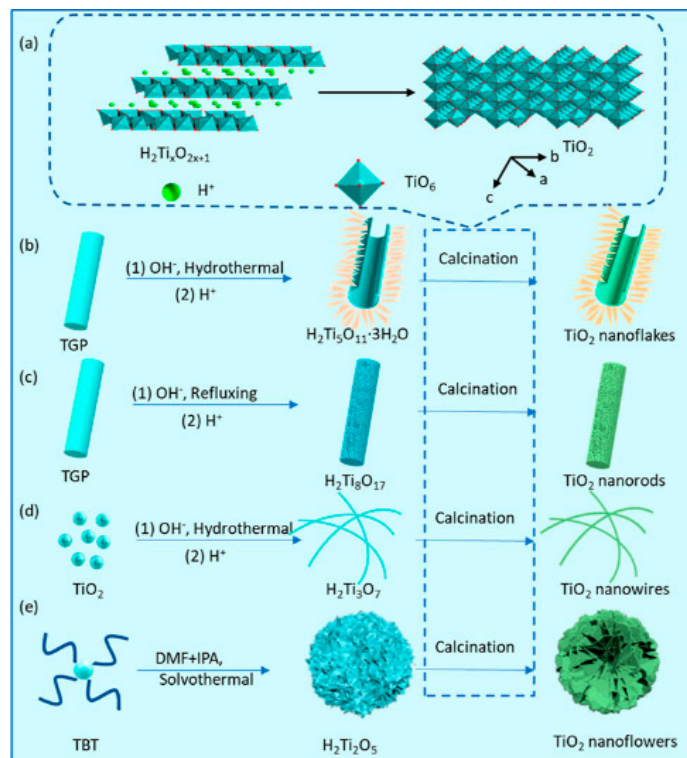


Figure 2. (a) Illustration for crystal phase transformation of TiO₂ from protonic titanate during the calcination process and illustration for the formation of different TiO₂ nanostructures from protonic titanate to: (b) TiO₂ nanoflakes, (c) TiO₂ nanorods, (d) TiO₂ nanowires and (e) TiO₂ nanoflowers [46]. Reprinted with permission from [46] Copyright 2022 American Chemical Society.

3.4. Light Harvesting

One of the limiting factors for TiO₂ photocatalysis is its narrow photocatalytic region, namely, due to its wider band gap, TiO₂ is UV-active. Further electronic structure modulation in TiO₂ photocatalysts can be performed by forming nanostructures, doping, co-doping, sensitizer doping, semiconductor coupling, heterojunction formation, oxygen vacancies formation, cocatalyst loading and defect engineering to transform it into a visible light active photocatalyst [60,61]. The band gap modification facilitates photoinduced charge separation and migration and improves the photocatalytic activity [14,62–65]. Wang et al. [66] reported the growth of nanorods and ultrathin nanowires on graphene aerogel for the formation of TiO₂ NR@GA and TiO₂ ultrathin NW@GA composites, where the graphene had a significant influence on the growth of TiO₂. Numerous influencing factors such as phase, morphology, size, band gap and intermediate energy levels were investigated as a function of heterogeneous interfaces.

4. Graphene in Photocatalysis: Benefits and Impacts

Graphene, a dream material, is an atom-thick sheet of sp²-hybridized carbon and has been in continuous use in scientific and engineering communities since its discovery [11–13]. One of the most fascinating applications of graphene is in designing heterogeneous semiconductor/graphene composite photocatalysts [14,15]. Heterogeneous photocatalysis is a promising and green process, well-known in the research community [16,17], since Fujishima and Honda discovered water splitting on TiO₂ photoelectrodes. To obtain high efficiencies in photocatalytic processes, photocatalysts

and their design are crucial, and most investigated photocatalysts include TiO₂ [18], g-C₃N₄ [19], Fe₂O₃ [20], ZnO [21], SnO₂ [22], and SnS₂ [23], CdS [67] CuO₂ [24], BiVO₄ [68], MoO₃ [25] and MoS₂ [69]. So far, most of the photocatalysts show poor stability and quantum yield and are rarely activated by visible light, posing a major challenge in the design of heterogeneous photocatalysts for practical applications. In this respect, composites based on graphene and semiconductors possess the potential to overcome these limitations, for instance, resulting in increased absorption in the visible range and higher photocatalytic activity [26].

The fundamental properties of a photocatalyst which influence a photocatalytic reaction are exceptional electrical conductivity and a strong electron-accepting ability, work function and chemical, physical and surface properties. These properties depend on the unique structure, interface and surface features, electronic structures, surface chemistry, charge transport, activation ability for certain reactants and molecular adsorption [2,27]. The properties of graphene can be tuned by suitable chemical modification, for instance, by controlling the level of oxidation which influences its electrical conductivity, or by its structural order [28,29]. Below, the intrinsic and tunable features of graphene and its role in a photocatalytic reaction are discussed.

4.1. Photocatalysis-Dependent Properties of Graphene

The performance of graphene and its derivatives varies with the nature of graphene, for example, with the level of oxidation which affects the electrical conductivity and semiconducting/semimetallic nature of graphene, the crystal structure and a variety of functional groups over its surface, and these aspects are discussed in detail below.

4.1.1. Crystal Structure

A crucial factor in photocatalysis is the electronic properties, which, for graphene, are exceptional due to its high-quality two dimensional crystal lattice. The band structure of graphene is rather unique and primarily consists of sp² hybridized carbon, where the valence orbital of the carbon consists of a 2p orbital (2p_z) perpendicular to the basal plane of graphene and three planar δ orbitals at 120° with each other. The hexagonal lattice of graphene is like a honeycomb and possesses two equivalent carbon sublattices per unit cell, referred to as A and B. The π electrons are delocalized in the conjugated network of carbon and are between the two adjacent carbons that are associated with π* (anti-bonding, the lowest unoccupied CB) and π (bonding, the highest occupied VB) bands [2]. These two bands meet at six points, known as neutrality or Dirac points. Due to the graphene's crystal symmetry, two points, K and K', which are independent of one another, can show the linear dispersion of orthogonal π and π* states without interactions in graphene. From the point of view of its electronic properties, the contact of the two bands at Dirac points further indicates that intrinsic monolayer graphene is a semimetal or zero-gap semiconductor [2,6]. In GO, an oxidized derivative of graphene, the VB maxima is composed of an O2p orbital rather than the usual π orbital present in graphene, and the CB minima is composed of an antibonding π* orbital [6].

4.1.2. Semimetallic Properties

Pristine graphene is a zero-bandgap, semimetallic material and therefore has a strong ability to accept electrons, which is a key point in promoting the activity of graphene-based photocatalysts. Specifically, in photocatalysis, graphene can accept, store and transfer photogenerated electrons and thereby can serve as an alternative electron sink/reservoir and a conductive support. Thus, graphene can extend the lifetime of photoinduced charge carriers, enhance charge separation and extraction and subsequently promote the photocatalytic activity of graphene-based photocatalysts [70]. These properties of graphene typically depend on an appropriate work function, in addition to the electrical conductivity. The contact barrier between a semiconductor and graphene can be controlled by the graphene's work function (please note that the latter determines the band alignment of

different materials). The work function of graphene increases with the increase in graphene layers and can be as large as that of graphite (≈ 4.6 eV) [71]. Furthermore, it can be changed by additional methods, such as introducing atomic defects (hole doping) [72] or doping (metal chloride, nitrogen) [73,74]. Moreover, the conductivity of graphene can be affected by the presence of sp^3 -hybridized carbon, the density of oxygenated groups present in the graphene nanosheets and the vacancy/defects that influence the electron density of states, thereby affecting the conductivity of graphene [75].

4.1.3. Semiconducting Properties

As discussed above, the nature of pristine graphene can be changed by its modification/oxidation. For instance, GO is the oxidized form of graphene, and the bandgap can be adjusted by tuning its level of oxidation. The electronic features of GO depend on its oxidation level, i.e., from pristine graphene, a semimetal, to GO, a semiconductor or an insulator [76]. Jung et al. [75] described the gradual change in GO (an electrical insulator) to graphene (a semimetal) during a thermal reduction process, thus showing an intimate relationship between the electrical properties and chemical structure of GO. The dependence of the GO's optical properties on its oxidation level was further confirmed [77,78]. Mainly, the presence of oxygen atoms bonded to carbon, the sp^3 bonds or/and the other defects are responsible for an energy gap in the density of electron states. The nature of the graphene/GO depends on the value of the bandgap. The RGO shows a gradual decrease in the optical band gap from 3.5 eV to 1 eV as the C/O ratio increases [79].

4.1.4. Electrical Conductivity

As mentioned before, graphene possesses exceptional electrical and electronic features due to the electrons confined in 2D geometrical symmetries. It is evident that semimetallic graphene has a high electrical conductivity, whereas GO is electrically insulating, and that the electrical conductivity can be controlled by the level of oxidation [80,81]. For example, this is indicated by the thermal or chemical reduction of GO, leading to a significant increase in conductivity as a result of the restoration of sp^2 carbon, as present in the graphitic network. The theoretical value of the charge carrier mobility for graphene is 2×10^5 cm²/Vs [82]. Below, in Table 1, the electrical conductivity of different graphene-based materials is listed with the corresponding references.

Table 1. An overview of the electrical conductivity of different graphene-based films/morphologies.

Material	Electrical Conductivity (S/m)	References
Graphite thin film (~ 3 μ m)	6120	[83]
Graphene (~ 3 μ m)	1750	[83]
RGO thin film (1.5 cm ²)	4.21×10^{-5}	[84]
GO thin film (1.5 cm ²)	4.57×10^{-5}	[84]
RGO (by nascent hydrogen)	12,530	[85]
RGO (by hydrazine)	2420	[86]
RGO (by aluminium)	2100	[87]
RGO (by HI)	30,400	[87]
RGO (N ₂ H ₄ and microwave reduction)	1180	[88]

The electrical properties of graphene can be improved by minimizing the role of different defects, which act as scattering centers and can inhibit the charge transport in graphene-based samples. During sp^2 carbon restoration, the partial removal of oxygen functionalities can result in the generation of defects which may affect the optoelectronic properties. For instance, RGO with more defects shows lower electrical conductivity as compared to an ideal monolayer of defect-free graphene [89]. The lower conductivity can also influence the charge transfer and separation during photocatalysis.

4.1.5. Surface Features

The properties of graphene vary with the functional groups attached to the graphene surface (e.g., GO has different functional groups: carboxyl, carbonyl, hydroxyl and epoxide [9]) as a result of the oxidation or modification/functionalization of graphene. The same is true for the specific surface area and density of defects in graphene sheets [90,91]. For a monolayer graphene, the theoretical value of the specific surface area is $2630 \text{ m}^2/\text{g}$ [92], whereas for monolayer GO, the estimated surface area is $2391 \text{ m}^2/\text{g}$ [93]. Esmaeili et al. [94] reported the specific surface area of GO as $\sim 53 \text{ m}^2/\text{g}$. These surface features can play a crucial role in the adsorption of targeted adsorbate and in redox reactions by photogenerated active species (e.g., charge carriers and reactive oxygen species) on the graphene materials, thereby improving the photocatalytic activity.

The unique two-dimensional honeycomb-like hexagonal graphene lattice offers a useful platform for forming composites with different nanostructured semiconductors, including quantum dots, nanowires/nanorods, nanosheets and porous structures, thereby favoring the formation of multifunctional graphene-based composite photocatalysts [95].

4.2. The Role of Graphene in Photocatalysis

In a photocatalytic system, graphene derivatives can act as a photocatalyst, a co-catalyst in most cases and/or as a photosensitizer [96], namely, as a photocatalyst because of its suitable bandgap that can absorb light and generate charge carriers to catalyze different species [97] and as a co-catalyst, owing to its unique electrical features and charge transport properties, thus allowing it to effectively sink/capture electrons from the semiconductor and to reduce photogenerated charge recombination [98]. When acting as a sensitizer, graphene and its derivatives are the main species that absorb light and initiate a photocatalytic process [98,99]. Below, we have further described the fundamental roles of graphene in photocatalysis.

4.2.1. A Photocatalyst Itself

Pristine GO, exhibiting a certain level of oxidation, can be also a semiconductor material and therefore can act as a photocatalyst itself [100], and when its bandgap lies in the range of 2.4–4.3 eV, it can be used for photocatalytic hydrogen generation in water [97]. As previously mentioned, an elevated degree of oxidation leads to an increase in the bandgap of GO, and a well-oxidized GO possesses the suitable CB maxima and VB minima for H_2 and O_2 evolution. For example, Yeh et al. [100] evaluated the photocatalytic properties of GO with different oxidation levels. Only the GO with the highest oxidation degree could generate O_2 , and other less oxidized GO, though with a sufficient bandgap, could not generate O_2 under light illumination. Please note that this is related to a typical phenomenon where GO undergoes reduction under light illumination, and therefore, the position of the VB minima can change. The GO with the highest oxidation degree was oxidized enough, and therefore, the VB minima remained positive enough for water oxidation under light illumination [100]. GO can act as a metal-free, eco-friendly and economical photocatalyst material; however, it has the key ability of suppressing its photocorrosion either by modifying GO (e.g., UV irradiation of GO causes its reduction, and after a certain time of exposure, the RGO is stabilized [99]) or by some other method.

4.2.2. A Cocatalyst

Graphene in photocatalysis is also very well-known for its role as a co-catalyst, as a substitute to the traditional costly noble metal co-catalysts. For example, in the case of RGO, when used with TiO_2 , its higher work function facilitates the charge transfer from TiO_2 to analyte or to generate reactive oxygen species [101]. Under the illumination of a composite based on RGO and TiO_2 , this facilitates the transfer of the photogenerated electron from the CB of TiO_2 to molecular oxygen. Such a process is used, for example, in the photo-oxidation of arsenic, and further investigation into the participating radicals by a competitive radical quencher test verified the simultaneous contribution from both the

hydroxyl and the superoxide radicals. Overall, the composite's results were similar to that of the common Pt/TiO₂ photocatalyst used in As(III) photo-oxidation [101].

4.2.3. A Sensitizer

Graphene can also act as a photosensitizer for visible light absorption in semiconductor-based photocatalysis, as it is an ideal support for charge transport in typical photocatalysts [102] (e.g., with ZnO [103], TiO₂ [99] and ZnWO₄ [99]). This occurs when GO is the main species that absorbs light, without affecting the bandgap of wide bandgap semiconductors such as TiO₂. The key aspect lies in its suitable bandgap for visible light activation, which makes it a potential macromolecular photosensitizer in a composite photocatalyst [10,97,100]. This leads to extended light absorption in the visible region, thereby resulting in promoted photocatalytic activity [96,99].

Therefore, it is clear that, in visible-light-driven photocatalysis, GO can also act as a photosensitizer. For example, Nasir et al. [10] illuminated a TiO₂/GO photocatalyst with a visible light source, where the GO acts as a sensitizer (by transfer of electrons to TiO₂ and by direct interaction of VB holes with water to initiate reactive oxygen species), which, in turn, degrades methylene blue (MB). Tismanar et al. [30] evaluated the visible light activity of GO in a thin film of TiO₂ and GO by degrading MB and imidacloprid. By large-scale DFT calculations, Du et al. [104] validated the direct photo-excitation of the upper VB electrons of graphene to TiO₂ CB under visible light illumination, which was also confirmed experimentally by the wavelength-dependent photocurrents of the similar photoanode. Zheng et al. [99] used GO as a photosensitizer in visible light driven hydrogen generation over TiO₂/GO, and the photoexcited electrons in GO were transferred to TiO₂, thereby reducing water to generate H⁺ and then H₂ gas.

In order to better elaborate and understand the role of GO as a cocatalyst or as a photosensitizer, an example of GQDs and TiO₂ heterojunction is included in Figure 3 [98]. In the case of a cocatalyst, the GQDs separate and transport charges and thereby prohibit charge recombination. The main species that absorbs light is TiO₂, from where the photogenerated electrons are injected into the CB of GQDs. The GQDs accept electrons and transfer them to the electrolyte to generate hydrogen gas. As a photosensitizer, the main species that absorbs light and generates photoexcited charge carriers is GQDs. The photogenerated electrons are then transferred to TiO₂ to further generate hydrogen gas [98]. Please note that the reported bandgap of GQDs in this case is 2.26 eV, and therefore, they act as a cocatalyst under UV illumination and as a photosensitizer for visible illumination.

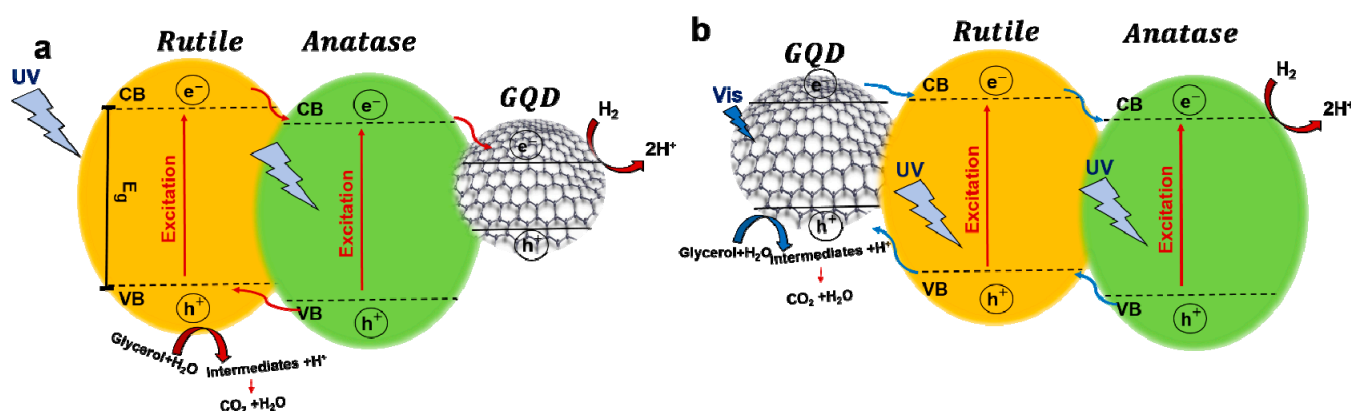


Figure 3. Role of graphene as (a) a cocatalyst and (b) a sensitizer in TiO₂/GQDs for improved photocatalytic H₂ evolution under solar light irradiation (Adapted from [98]. Reprinted with permission from [98] Copyright 2020 American Chemical Society).

5. Design of Composite Graphene/TiO₂ Photocatalysts

There are various techniques used for the synthesis of graphene–TiO₂ nanocomposites [1,105,106]. In most, either (i) commercial/pre-synthesized TiO₂ is mixed with graphene or its derivatives by sonication [107] or by simple mixing followed by photoreduction [1,108,109], or (ii) a graphene derivative is used as a support to immobilize and grow TiO₂ nanostructures (e.g., the hydrothermal method [110,111], solvothermal method [106,112], sol gel [113,114], electrodeposition [115–117] etc.). However, there is no optimal method that is well-known for the synthesis of these composite structures, and the quest for a more suitable, scalable and refined method is still in progress and the focus of researchers. Recently, Nasir et al. [10] introduced a one-step, UV-induced photocatalytic synthesis of TiO₂/GO composites. The composites obtained could be directly used for visible-light-driven photocatalysis. Below, in Table 2, we have summarized some of the most recent trends in the design of such graphene-based TiO₂-mixed composites, taking into account the starting Ti material, graphene derivatives and resulting photocatalysts in view of the synthesis method used and of the resulting morphology.

Table 2. An overview of the recent methods for the design of graphene-based/TiO₂ composites.

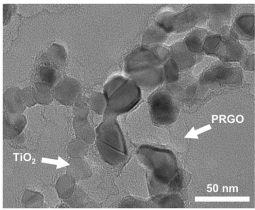
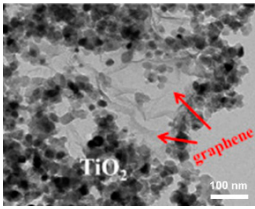
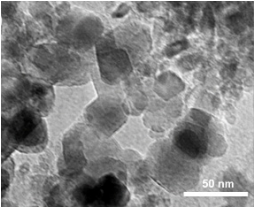
Ti Precursor	Graphene Derivative	Photocatalyst	Synthesis Method	Morphology	Reference
Commercial P25	Pre-synthesized GO	Photoreduced GO/TiO ₂	Simple mixing, followed by photoreduction	 <p>PRGO TiO₂ 50 nm</p>	a. [3]
TiCl ₄	RGO seeded on TiO ₂ nanocrystals	Durian-like mischcrystal TiO ₂ /graphene	Seed-induced hydrothermal approach	Uniform growth of durian-like compact clusters of TiO ₂ on RGO surface	[8]
Commercial TiO ₂	Sulphonated RGO GO by Hummer's method	Edge-sulphonated graphene-decorated TiO ₂	Ultrasonic self-assembly method	 <p>graphene TiO₂ 100 nm</p>	b. [118]
Commercial TiO ₂ anatase	Commercial GO	TiO ₂ nanorod array on a 3D GO framework	Hydrothermal	Uniformly dispersed TiO ₂ nanorods (l = 200 nm, d = 30 nm) anchored on a 3D GO framework	[119]
TiO ₂ (P-25)	GO by modified Hummer's method	TiO ₂ /graphene aerogel	Hydrothermal	 <p>50 nm</p>	c. [120]

Table 2. Cont.

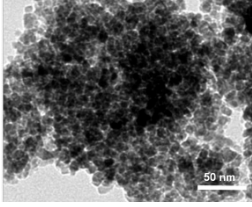
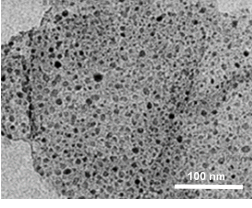
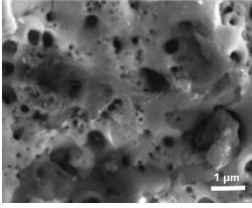
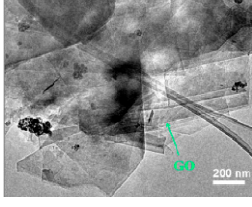
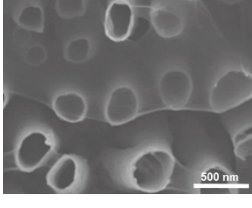
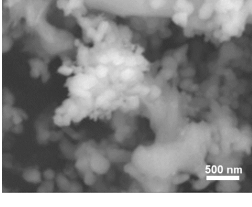
Ti Precursor	Graphene Derivative	Photocatalyst	Synthesis Method	Morphology	Reference
Titanium (IV) isopropoxide (TTIP)	GO by Hummer's method	1 wt%RGO/S _{0.05} N _{0.1} TiO ₂ nanocomposite	Solvothermal		d. [121]
TTIP	GO by modified Hummer's method	RGO-15%TiO ₂	Hydrothermal		e. [92]
TiO ₂ by microwave-assisted synthesis Precursor: TTIP	GO by Tour's method, amine-modified GO	GO and amine-modified GO/TiO ₂	Hydrothermal	No SEM shown	[122]
Ti substrate	RGO	Tungsten-doped TiO ₂ /RGO	Plasma electrolytic oxidation		f. [123]
Grey TiO ₂ Precursor: TiO ₂ (P-25)	Graphite	Grey TiO ₂ /GO	UV induced photolysis		g. [10]
TiO ₂ nanotubes by electrochemical anodization	GO	Pt coated, GO wrapped TiO ₂ nanotubes	Electrophoretic deposition		h. [124]
Commercial TiO ₂	GO by Hummer's method	TiO ₂ /RGO	Hydrothermal		i. [12]

Table 2. Cont.

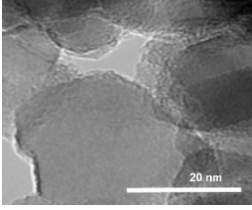
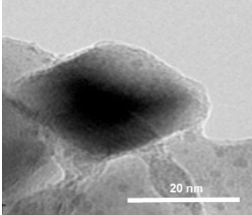
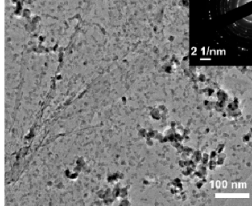
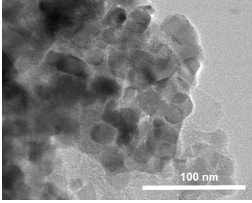
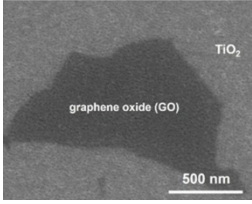
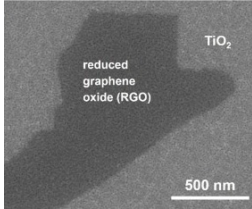
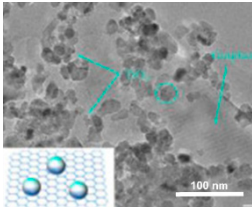
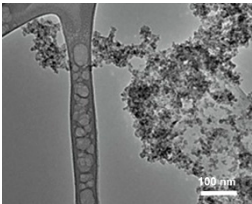
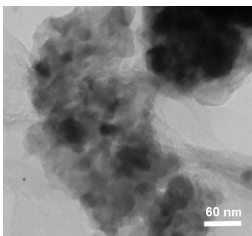
Ti Precursor	Graphene Derivative	Photocatalyst	Synthesis Method	Morphology	Reference
Commercial TiO ₂	GQDs by hydrothermal method Precursor: SWCNTs	Graphene quantum dots anchored TiO ₂	Simple mixing		j. [125]
	GQDs by hydrothermal method Precursor: Carbon fiber				
Precursor: Tetrabutyl titanate (TBOT)	Commercial Graphene	Black TiO ₂ /graphene composites	Sol gel		k. [126]
TiO ₂ (P-25)	GO by modified Hummer's method	TiO ₂ /GO	Hydrothermal		l. [127]
Precursor: Titanium (IV) butoxide	Commercial GO	TiO ₂ /GO	Sol-gel	Agglomerated and distributed growth of TiO ₂ nanoparticles over the GO surface	[128]
TiO ₂ coating by sol-gel dip coating method Precursor: TTIP	Commercial GO suspension	TiO ₂ /GO	Dip-coating		m. [129]
		TiO ₂ /RGO	Chemical reduction of dip-coated TiO ₂ /GO sample		

Table 2. Cont.

Ti Precursor	Graphene Derivative	Photocatalyst	Synthesis Method	Morphology	Reference
Ca-doped TiO ₂ by hydrothermal method Precursor: TBOT	Exfoliated graphene	Ca ²⁺ -doped mixed-phase TiO ₂ /graphene	Electrostatic self-assembly process/ Sonication-assisted mixing		n. [130]
TiO ₂ Precursor: TTIP	Few-layer graphene by mechanochemical method	Few-layer graphene TiO ₂	Mechanochemical synthesis		o. [131]
TiO ₂ by sol-gel method Precursor: TTIP	GO by modified Hummer's method	TiO ₂ supported-RGO	ultrasonic-assisted solvothermal method		p. [132]

a. Reprinted with permission from [3] Copyright 2022 Elsevier Ltd. b. Reprinted with permission from [118] Copyright 2022 Elsevier Ltd. c. Reprinted with permission from [120] Copyright 2022 Elsevier Ltd. d. Reprinted with permission from [121] Copyright 2022 BioMed Central Ltd. (Part of Springer Nature). e. Reprinted with permission from [92] Copyright 2022 Elsevier Ltd. f. Reprinted with permission from [123] Copyright 2022 Elsevier Ltd. g. Reprinted with permission from [10]. Copyright 2022. h. Reprinted with permission from [124] Copyright 2022 Elsevier Ltd. i. Reprinted with permission from [12] Copyright 2022 Elsevier Ltd. j. Reprinted with permission from [125] Copyright 2022 MDPI. k. Reprinted with permission from [126] MDPI. l. Reprinted with permission from [127] Copyright 2022 Elsevier Ltd. m. Reprinted with permission from [129] Copyright 2022 Elsevier Ltd. n. Reprinted with permission from [130] Copyright 2022 Elsevier Ltd. o. Reprinted with permission from [131] Copyright 2022 Elsevier Ltd. p. Reprinted with permission from [132] Copyright 2022 Elsevier Ltd.

6. Characterizing Composite Photocatalysts of Graphene/TiO₂

Of the existing characterization techniques, the ones that are the most used for confirming the presence and for characterization in view of evaluating graphene in TiO₂/graphene photocatalysts are: (i) Raman spectroscopy for the presence of graphene, graphite and the typical structural characterization of TiO₂ [133,134], (ii) Fourier-transform infrared spectroscopy (FTIR) for molecular groups and chemical bonding (only specific molecules can be detected) [135], (iii) X-ray photoelectron spectroscopy (XPS) for chemical and compositional properties of the material's surface [136] and (iv) scanning electron microscopy (SEM) and transmission electron microscopy (TEM), coupled with elemental mapping, for evaluating morphology (atomic scale structural information and interactions with the support is also possible with TEM coupled with elemental composition) [137].

6.1. Raman Spectroscopy

Raman spectroscopy is a powerful surface sensitive tool used to study the structure of the composites, giving information related to their structural characterization. For carbon-based materials, it stands as a high-resolution tool enabling the characterization of the lattice structure and the electronic, optical and phonon properties [133,134]. The Raman spectra of anatase TiO₂ typically show four peaks at 148, 398, 514 and 641 cm⁻¹, attributed to E_{g(1)}, B_{1g(1)}, A_{1g} + B_{1g(2)} and E_{g(2)} vibrations, respectively [138]. In the case of graphite or graphene-based materials, Raman spectra provide detailed structural data

related to the G and D bands [133,139]. For example, for GO, the usual peaks observed are: (a) for the D band (disorder/sp³ carbon), usually at ~1350 cm⁻¹, and (b) for the G band (sp² carbon), at ~1580 cm⁻¹ [140], and pure graphite does not show a clearly evident D band [141]. Generally, a higher disorder in the lattice results in broadening of the G and D bands, and a higher relative intensity of the D band compared to the G band (evaluated by their intensity ratio, the I_D/I_G ratio). The Raman spectrum of GO shows not only a higher I_D/I_G ratio but also a blue shift in the peak position of the G band compared to that of graphite [141]. Nasir et al. [10] observed the gradual emergence of the D band with an increase in the GO's oxidation level, hence revealing an interesting fact, that GO with more oxygenated groups results in a higher I_D/I_G ratio. With the increase in the D band's intensity, additional characteristic disorder-related peaks appear, i.e., D + D', 2D and D' for the more oxidized GO [10]. The D + D' band (also referred as D + G) appears as a bumpy peak at ~2940 cm⁻¹ and can be observed in highly defective polyaromatic structures [142]. The 2D band appears due to physical defects (i.e., edge defects in graphene sheets), and a D' peak appears at ~1620 cm⁻¹ and can be related to any type of defect [10,142]. In contrast to TiO₂/graphite composites, for TiO₂/GO, a more intense and broader G band is observed, and this is typically used to confirm the formation of GO [10]. Cham sa-ard et al. [140] evaluated the difference in the Raman spectra of GO and RGO, and namely, the I_D/I_G ratio for GO and RGO was 1.02 and 1.17 due to the loss of oxygenated functional groups. Shahrezaei et al. [138] used Raman spectroscopy to confirm the presence of a modified form of graphene decorated on TiO₂ multileg nanotubes, and the authors verified the presence of the D and G bands in the composite, which were absent for the pristine nanotubes.

More interestingly, Liu et al. [143] used a TiO₂ nanosheet as a support to directly grow graphene, and Raman spectroscopy was used to observe the growth phenomena as a function of the growth time, as shown in Figure 4. The D and G bands, typical characteristics of carbon materials, became more pronounced after 2 h (180 min), as seen in Figure 4a (inset I), where intense D and G bands can be observed together with the appearance of the 2D and D + G bands, as well as with an increase in the D band. A sharp change in the FWHM of the G band was measured at 0.5 h (30 min) as a result of the complete formation of a graphene monolayer, with no further drastic change [143]. Nasir et al. [10] observed a sequential increase in the I_D/I_G ratio as a function of graphite oxidation (directly dependent on the UV illumination time, which led to a gradual increase in graphite oxidation), as indicated in Figure 4b.

The above are the most critical aspects of how graphene-based materials in a metal oxide composite can be identified by Raman spectroscopy and of what to expect with respect to their different oxidation level, particularly at trace concentrations of graphene-based materials. However, the main and initial fingerprint for the presence and investigation of GO or its modified forms is therefore the appearance of the D and G bands and the I_D/I_G ratio.

6.2. FTIR Spectroscopy

Fourier-transform infrared spectroscopy (FTIR) is typically used for the identification of chemical composition or molecular structure, specifically to identify the chemical bonds and characteristic functional groups present in a material or a composite [144,145]. In graphene-based materials, the extent of oxidation and the presence of oxygenated species can be evaluated from its FTIR spectra. FTIR also provides information with respect to the surface reactive sites of a material and their interactions with certain species [146]. FTIR spectroscopy is typically the second preferred characterization technique used to identify the presence of GO in composites [146,147]. Figure 5 shows a very clear overview of typical FTIR spectra for GO and its composites with TiO₂ [148]. A typical IR spectrum of GO shows a broad band between 3600–3200 cm⁻¹ along with a band at 1400–1200 cm⁻¹ corresponding to –OH groups, at ~1700 cm⁻¹ for carbonyl groups, 1600–1400 cm⁻¹ for the C=C of graphene, 1100–1000 cm⁻¹ for alkoxy groups and ~950 cm⁻¹ for epoxy groups [9]. For TiO₂, bands attributed to –OH groups are present, along with Ti–O/Ti–O–Ti peaks in the ~900–400 cm⁻¹ region [149]. In the case of the GO/TiO₂ composites, overlapped

spectra are observed. The main peaks taken into account for the identification of such composite are: (i) -OH groups ($3200\text{--}3600\text{ cm}^{-1}$, $1400\text{--}1200\text{ cm}^{-1}$), this is usually observed in pristine anatase and (ii) a Ti-O-C peak, with a blue shift in the wavenumber compared to the Ti-O/Ti-O-Ti peak [148,150]. In $\text{TiO}_2\text{-RGO}$ composites, the loss of functional groups in the RGO results in less peaks in the spectra compared to the GO composite [148,150]. It is important to note that, in most composites with titanium dioxide, the amount of GO is quite low, and therefore, in the corresponding IR spectra, the functional groups of GO are retained with a significant decrease in peak intensity [148,151]. Sim et al. [152] observed the loss of the C-O peak at 1220 cm^{-1} , ascribed to the interaction of the epoxide/phenolic groups of GO with -OH groups in the Ag/TiO_2 nanotubes, thereby forming Ti-O-C bonds in their composites with GO (the absorption peak for Ti-O-C in combination with Ti-O-Ti vibration appeared at 800 cm^{-1}).

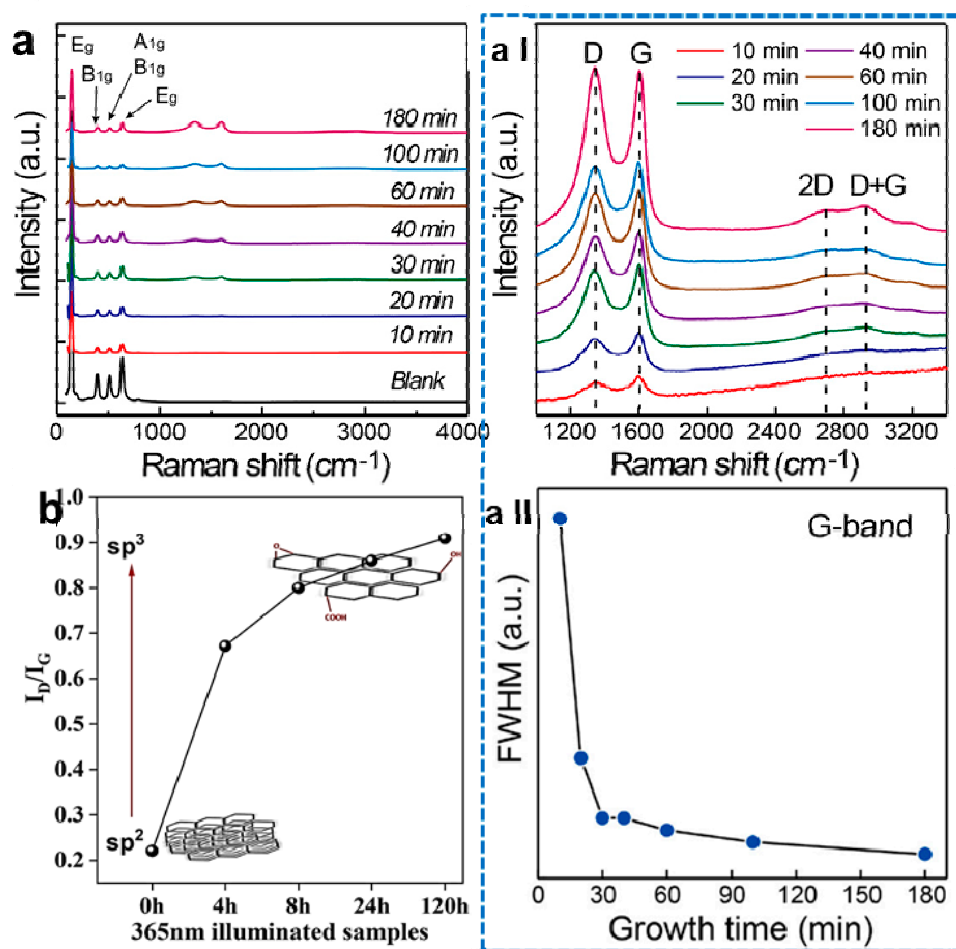


Figure 4. (a) Raman spectra of a series of $\text{TiO}_2/\text{graphene}$ samples prepared at different growth times, and the inset includes the (I) expanded view of spectra in the range of $1100\text{--}3300\text{ cm}^{-1}$, and (II) the plot of the FWHM of the deconvoluted G band as a function of growth time [143] (Reprinted with permission from [143] Copyright 2018 American Chemical Society); and (b) the I_D/I_G ratio as a function of increases in oxidation level (subjected here with increases in time) of GO in the composite [10] (Reprinted with permission from [10] Copyright 2022 John Wiley & Sons, Inc.).

6.3. XPS Spectroscopy

X-ray photoelectron spectroscopy (XPS) is one of the most used characterization techniques, establishing the chemical and compositional properties of surfaces, with a high surface sensitivity. XPS is also widely used for the evaluation of graphene-based materials [153,154] or various graphene-based composites with semiconductor oxides [155,156]. Moreover, up to now, the adventitious carbon peak is typically used

for spectra calibration, and more recent reports have shown the drawbacks of such an approach and how to further proceed in order to allow for reliable determination of the chemical states [136,157,158], as well as for accurate peak fitting [157,158].

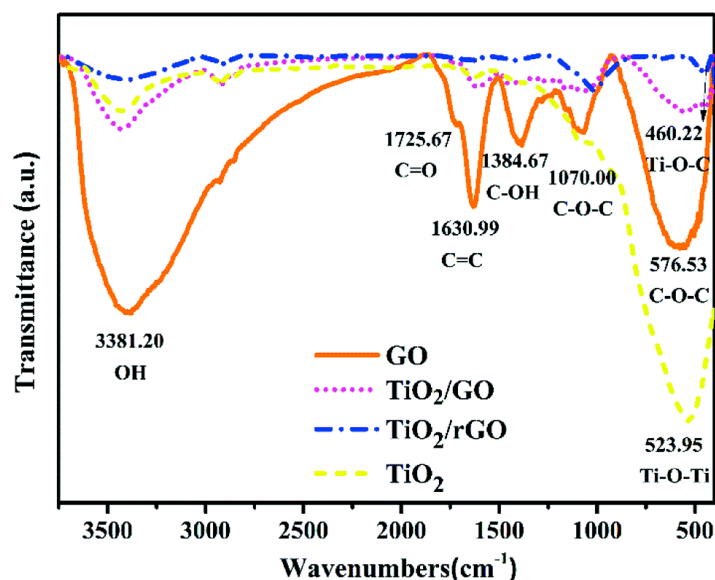


Figure 5. FTIR spectra of as-obtained GO and TiO₂, and of the corresponding TiO₂ composites after the incorporation of GO or rGO [148] (Reprinted with permission from [148] Copyright 2018 Royal Society of Chemistry).

Typically, the C1s peak of graphene-based materials (graphite, graphene and graphene oxide) consists of the peaks discussed below: (i) for graphite, an sp² peak at 284.1–284.8 eV (showing an asymmetric peak shape) [158–161], C-OH groups at 285.6 eV and C-O groups at 286.6 eV due to atmospheric oxidation [141], as well as a shake-up feature related to the pi to pi* transition observed around 290.5–291 eV [158,161,162]; and (ii) for graphene/graphene oxide, an sp³ peak at 284.6–285.1 eV (typically 1 eV higher than the sp², [113] C-O at 286.4–286.6 eV (epoxide groups), C=O at 288.2 eV and COOH groups at 289.2 eV [158,163,164]. For this, there is also the presence of adventitious carbon at 284.8 eV.

When evaluating graphene-based composites containing TiO₂, spectra evaluation can also include the Ti2p peak, and when changes occur to the structure of the graphene-based materials, i.e., to the C1s peak position and shape, peak calibration can be performed with the former. In this respect, Nasir et al. [10] obtained GO by the UV illumination of grey TiO₂/graphite nanocomposites, and XPS confirmed the conversion of graphite to GO. Figure 6a–c show the high resolution C1s, Ti2p and O1s peaks of pure graphite powder and of the 0, 4, 8, 24 and 120 h UV illuminated grey TiO₂/graphite composites. The presented XPS peaks clearly validate the changes occurring in the C1s peak (switch from graphite to GO), as well as the decrease in the surface coverage of GO with grey TiO₂ nanoparticles, with increasing the UV illumination time (with more illumination time, an increase in the intensity of the Ti2p and O1s peak is observed, together with a decrease in the C1s peak intensity) [10]. The peak fitting of the pure graphite was in line with data from the literature [158–160]. The 24 h UV-illuminated nanocomposite (Figure 6d) confirmed an sp³ contribution at 285.2 eV due to oxidized graphite (together with peaks attributed to C-O at 286.4 eV, for epoxide groups C=O at 288.16 eV and COOH groups at 289.2 eV) [10].

Similarly, Kumari et al. [156] evaluated the chemical state variations of GO/TiO₂ nanocomposites, and in addition to confirming the presence of TiO₂ (Ti2p_{3/2} at 458.8 eV), the authors performed detailed investigations of the O1s and C1s peaks. Namely, the peak fittings for the O1s and C1s were confirmed in the case of the O1s peak for the C=O and C-OH functional groups at 531.4 eV and 533.6 eV, respectively, [156,165], and for the C1s

peak, there were weaker residual oxygen-containing functional group peaks compared to C=C (confirming the partial reduction of GO during composite formation) [156,166].

Rajender et al. [167] evaluated the changes in the mixed hybrid of TiO₂ and GO quantum dots (QDs) by investigating the C1s and O1s peaks. The fitted peaks (Figure 6e–h) showed the relocation of oxygenated groups after the formation of the hybrid, i.e., the C-O (ether) and COOH functional groups were significantly reduced in the hybrid sample, meaning that some of the oxygen-related functional groups may have been converted to in-plane epoxy groups to facilitate the possible formation of C-O-Ti bonds in the TiO₂-GQD hybrid, observed also in the O1s peak fitting in the peak at 531.7 eV.

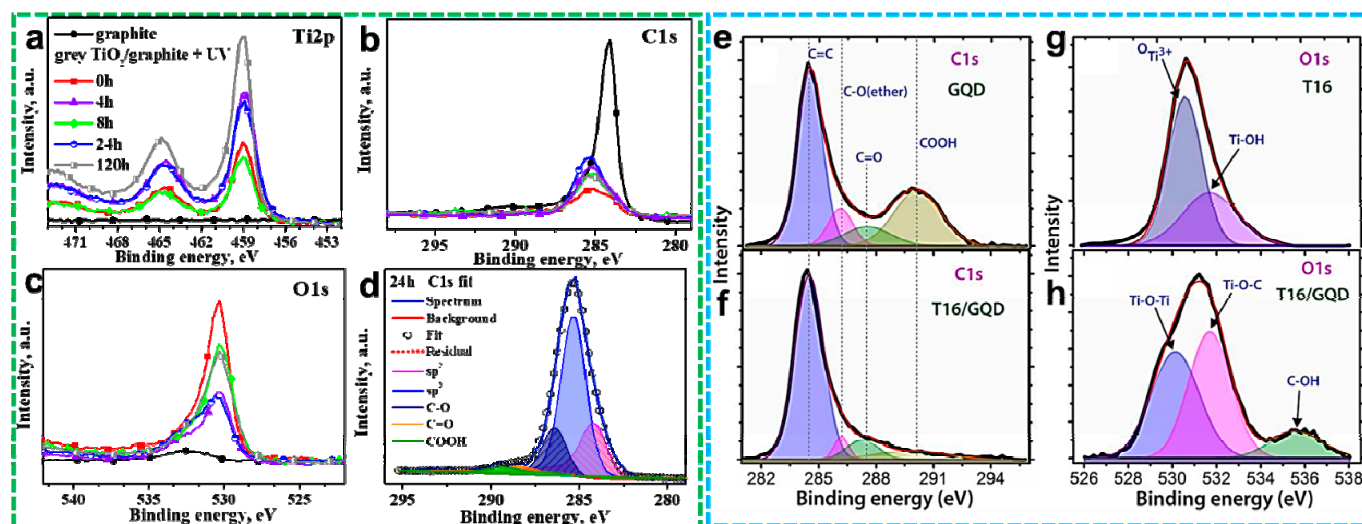


Figure 6. High-resolution XPS analysis: (a–c) raw data of Ti2p, C1s and O1s peak of the TiO₂-GO composite (increases in time show oxidation level of GO), (d) C1s spectra of 24 h UV-illuminated composites [10] (Reprinted with permission from [10] Copyright 2022 John Wiley & Sons, Inc.), Composites of GO quantum dots (gQD) and TiO₂ (T16) with the corresponding peak fittings for the (e,f) C1s spectra (GQDs and the T16/GQD composite) and the (g,h) O1s spectra (T16 and T16/GQD) [167] (Reprinted with permission from [167] Copyright 2018 Elsevier Ltd.).

6.4. SEM and TEM

Scanning electron microscopy (SEM) is extensively used for evaluating the nanostructure and morphology of various materials, both in top-views or in cross-sections, whereas transmission electron microscopy (TEM) enables the detailed evaluation of atomic-scale structural information [137].

For example, SEM is generally used to study and confirm the presence of graphene sheets in composites. The morphology of TiO₂ can vary from 0D nanoparticles, to 1D-nanotubes/nanowires, to 2D-nanosheets. Note that pristine graphite has a thick, layered and non-transparent structure. At a magnification of 5–50 k, many stacks can be found with a much bigger particle size of graphite flakes, whereas GO has a smaller particle size, and only few stacks can be found at 40–300 k (see Figure 7). This is because GO is produced by oxidation, and thereby the exfoliation of graphite structure leads to isolated mono- or multilayer sheets of graphene [168].

The GO can, therefore, be characterized by crumpled, silk-veil-like, thin nanosheets present with the TiO₂ nanostructures. In the case of composites with TiO₂ nanoparticles, well-defined, mono or multilayer sheets of GO decorated with TiO₂ nanoparticles and agglomerates can be clearly observed [169], as seen in Figure 8a. Trapalis et al. [79] observed 2–6 layered sheets of graphene in the TiO₂ nanoparticle/graphene composites (the graphene content was only 1%). When combined with spaced TiO₂ nanotubes [138] (showing distinct spacing in between the tubes compared to the classical close-packed nanotubes [170]), the graphene sheets were found on the top surface and in between the nanotubes as well, as

seen in Figure 8b. In Figure 8c,d, SEM images of TiO₂/RGO with 5% RGO concentration have been included together with the as-obtained elemental analysis, confirming the presence of carbon [171].

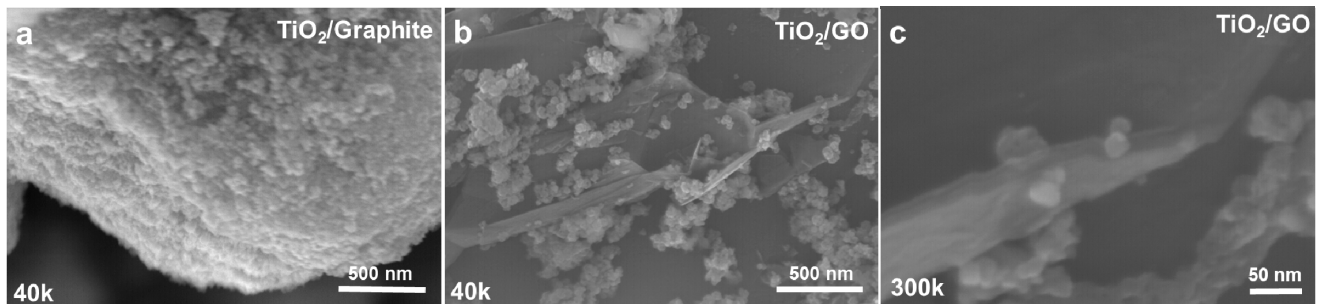


Figure 7. SEM images at a magnification of 40 k for (a) TiO₂/graphite and (b) TiO₂/GO, and at a magnification of 300 k for (c) TiO₂/GO (c. Reprinted with permission from [10] Copyright 2022 John Wiley & Sons, Inc.).

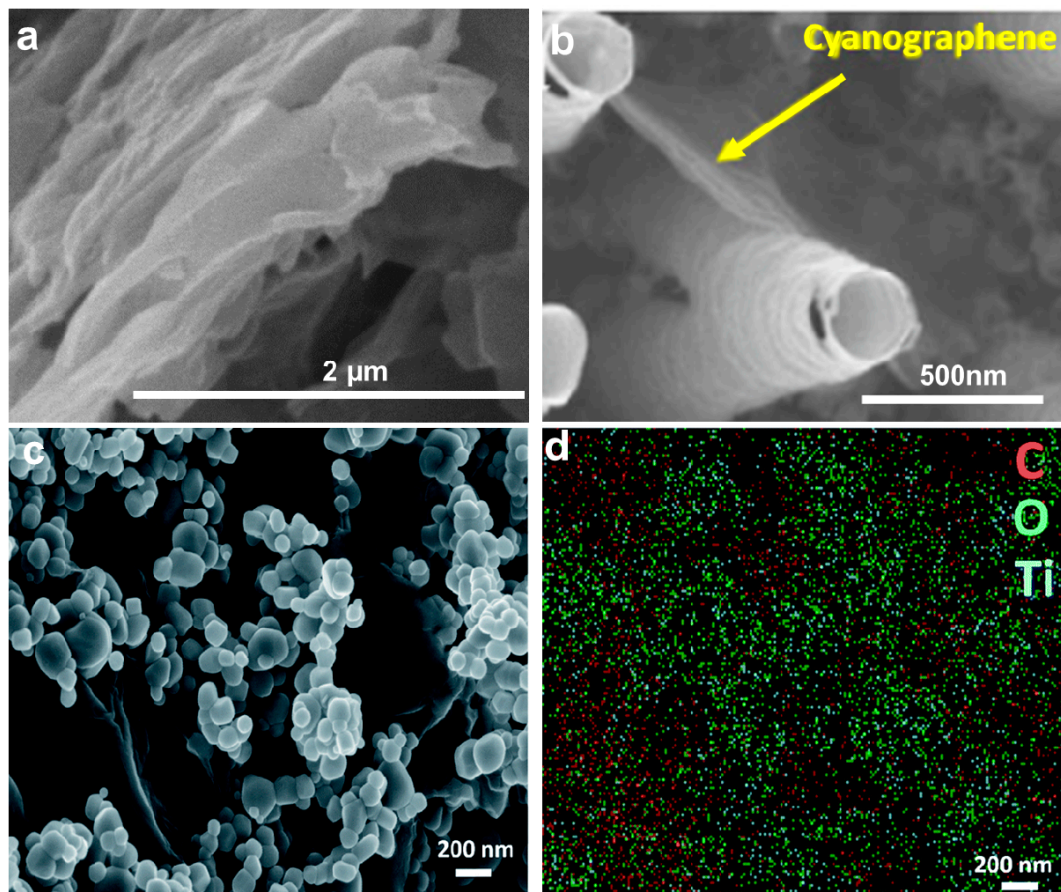


Figure 8. SEM images of (a) GO nanosheets [9] (Reprinted with permission from [9] Copyright 2020 Elsevier Ltd.) and (b) the anodized spaced TiO₂ nanotubes with wrapped-around and modified nanosheets of graphene [138] (Reprinted with permission from [138] Copyright 2020 MDPI); (c) TiO₂-RGO (5%); (d) EDS elemental mapping of the area shown in (c) [171] (c,d—Reprinted with permission from [171] Copyright 2020 Royal Society of Chemistry).

TEM is an essential tool in the analysis of graphene-based nanosheets for more detailed morphology insight into the nanosheets and for the confirmation of the GO's nanoscale features. For instance, in Figure 9, very translucent, wrinkled nanosheets of GO can be clearly observed, and the inset in Figure 9b shows that the GO's sheet thickness is in

the nanometer range. Well-dispersed TiO₂ nanorods can be seen on the GO sheet in Figure 9b [172]. The lattice spacing of GO can also be estimated by TEM; for example, Nasir et al. [10] obtained a lattice spacing of 0.35 nm (002) for GO and 0.35 nm (101) for the TiO₂ region.

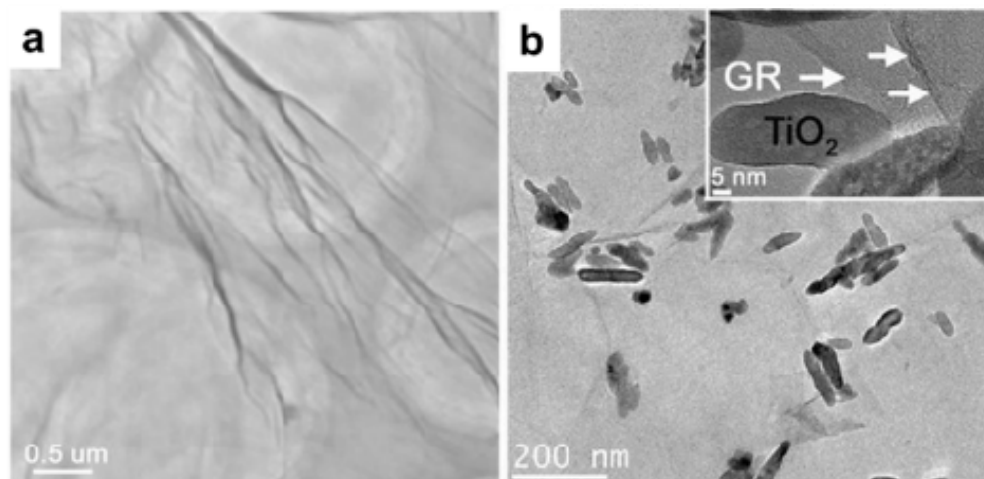


Figure 9. TEM images of (a) GO and (b) 0.1-TiO_{2-x}/GR composite [172] (Reprinted with permission from [172] Copyright 2014 Springer Nature Ltd.).

6.5. UV-Vis Spectroscopy

UV-Vis analysis is a simple analytical method for quantitative analysis and for evaluating the molecular level mechanisms in a chemical compound/material, and it can also estimate band gaps and evaluate the optical properties of the materials [173]. UV-Vis spectroscopy does not give a direct mark for the presence of graphene or GO; however, it proves useful in evaluating the extended range of light absorption in the visible region, which is a usual characteristic of graphene-based semiconductor composites. The typical characteristic features observed for identifying GO are: (i) a shoulder attributed to $n-\pi^*$ plasmon peak, which usually appears at ~ 310 nm [174] and (ii) a $\pi-\pi^*$ plasmon peak between ~ 230 – 300 nm for graphene, or at ~ 230 nm for well-oxidized graphene [175], [174]. In graphene-based materials, the $\pi-\pi^*$ absorption peak corresponds to the sp^2/sp^3 character. The amount of shift in the position of this peak towards the visible range corresponds to the increase in the sp^2 character, thereby increasing the growth of the number of sp^2 layers [175].

Figure 10a includes the UV-Vis spectra of GO and RGO, and the main absorption edge at 226 nm was shifted to 262 nm after reduction. This red shift suggests the restoring of the electronic conjugation in the graphene sheets after reduction [176]. Mixed composites show a red shift towards longer wavelengths and an increase in the visible range absorption compared to pristine TiO₂, as seen in Figure 10b, where TGPPC_x stands for the TiO₂ graphene photocatalyst and x stands for the content of graphene [175]. A modified form of graphene (cyano graphene, cyano platinized graphene), when decorated on the TiO₂ nanotubes, showed a red-shift (ca. 10–20 nm) in the absorption edge and relatively more absorption in the visible range of light than the bare TiO₂ nanotubes [138]. Zhang et al. [177] observed a 30 nm red shift in the absorption edge of a layer-by-layer composite of TiO₂ and graphene. In this case, a strong visible range absorption was also observed, indicating high photocatalytic activity in the UV and visible range. Similarly, Rong et al. [175] observed a red shift in the TiO₂ absorption spectrum, as a function of the graphene content with a decrease in the band gap, especially at a higher graphene content.

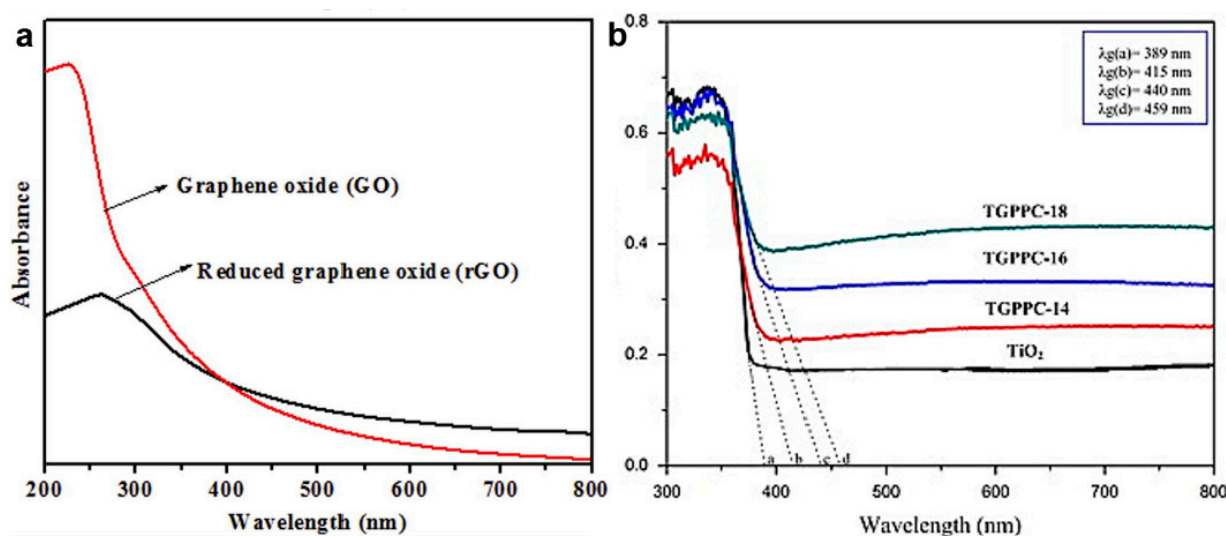


Figure 10. Comparison of UV-Visible spectra of (a) aqueous solutions of GO and RGO [176] (Reprinted with permission from [176] Copyright 2017 Elsevier Ltd.) and (b) mixed composites with different content of graphene [175] (Reprinted with permission from [175] Copyright 2015 Elsevier Ltd.).

7. TiO₂—Graphene Composites: Current Status and Applications

TiO₂ photocatalysis has made several breakthroughs in various practical and industrial applications, primarily in the field of environmental safety (e.g., wastewater treatment, air purification, microorganism inactivation/sterilization, etc.). As previously mentioned, an ideal photocatalyst represents outstanding features such as economical features, environmentally benign features, long-term stability, reproducibility, recyclability and efficient photocatalytic activity [178]. Despite several advantages of TiO₂ photocatalysts, there are some limitations, such as (a) recyclability, which is relevant to separation and recovery, (b) narrow regions of light harvesting due to its wide band gap, (c) faster recombination of photogenerated carriers, (d) low surface area, (e) less adsorption capacity and (f) aggregation issues [179]. Countermeasures usually include, for example, the modification, optimization, design and development of a TiO₂ photocatalyst to improve photocatalytic efficiency, stability, reproducibility and recyclability [126,180,181].

Graphene-based TiO₂ composites have emerged as efficient photocatalysts [1,6,182–186] for the next generation photocatalytic applications [1,105,187–192]. The synergistic effect between components in ternary photocatalysts (comprising three components, where each photocatalyst component plays its potential role to maximize the photocatalytic activity) offers significant merits, such as multiple interfaces, improved separation and migration/transfer of charges, reduced recombination of photogenerated charge carriers, prevented agglomeration, high specific area and high stability [193]. Recent progress in the development of TiO₂/graphene-based photocatalysts in various applications, such as wastewater treatment for the removal of pollutants, air purification, water splitting for hydrogen production, dye-sensitized solar cells (DSSCs), photoconversion of CO₂ into renewable fuels, NO_x fixation and deactivation of microorganisms (see also Figure 11), is further discussed in this section.

7.1. Remediation of Water

Typical water contaminants include sewage industrial effluent (e.g., textiles, paper, pharmaceutical industry, etc.) and domestic contaminants (e.g., detergent, pharmaceuticals, pesticides, etc.) [194]. The incorporation of graphene in TiO₂ results in a good adsorbent for the removal of organic pollutants (e.g., dyes, phenolic compounds, chlorinated products, antibiotics, pesticides and crude oil) and microbial inactivation due to electrostatic attraction, π – π interaction, visible light absorption and larger electron mobility [195–200]. TiO₂/graphene-based composites have revealed their potential as cost effective, envi-

ronmentally friendly and sustainable photocatalysts in support of wastewater treatment technology for the degradation of organic pollutants and environmental remediation [200].

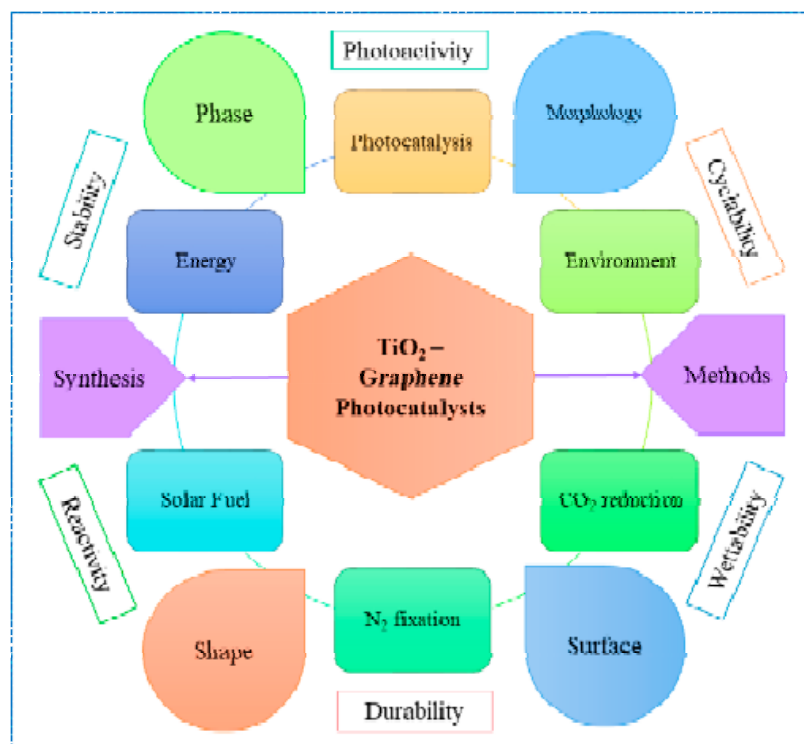


Figure 11. Schematic representation of titania-graphene composites.

An example of such a wastewater treatment application is for xanthate degradation (xanthane is an environmental pollutant resulting from the mineral industry, i.e., from the mineral flotation process, and is toxic for biota [201]). The photodegradation efficiency of an 18% TiO₂/G composite under simulated light irradiation was reported as 97.03% after 100 min, much higher than for pure TiO₂ (17.88%). This is attributed to an extended photoresponse in the composite material from 200–380 nm to 200–800 nm [127]. Similarly, high photocatalytic degradation was observed for TiO₂/GO composites for picric acid (also known as 2,4,6-trinitrophenol, which is a dangerous nitroaromatic environmental pollutant generated from dye, leather and chemical industries, having low biodegradability and high toxicity [202]) [12]. RGO-nano TiO₂ composite (RGO-nTiO₂) showed 88% degradation efficiency for metachrome yellow dye (or alizarin yellow GG, an azo dye which is textile effluent, highly toxic and carcinogenic [203,204]) under natural sunlight with 80% efficiency, higher than for that of plain TiO₂. The enhanced efficiency was attributed to the superoxide anion radical that played the key role in pollutant oxidation [20]. The Z-scheme photocatalytic composite g-C₃N₄/RGO/TiO₂ showed an efficient performance for ammonia-nitrogen removal from water. Ammonia-nitrogen is a toxic groundwater pollutant, and its impact is widespread, as its excessive quantity causes malodor in river water that can lead to eutrophication, weakening of the self-depuration capability of water and threats to public health. Heavily polluted waters contain an ammonia-nitrogen level of >15 mg/L, and a minor pollution level is considered to be 8–15 mg/L [205,206]). The photogenerated electrons from the TiO₂ conduction band can transfer to the g-C₃N₄ valence band by the Z-scheme mechanism. These electrons recombine in g-C₃N₄ with photogenerated holes. The g-C₃N₄/RGO/TiO₂ Z-scheme system shows improved redox capacities for NH₃-N oxidation and NO³⁻ reduction (Figure 12) [207].

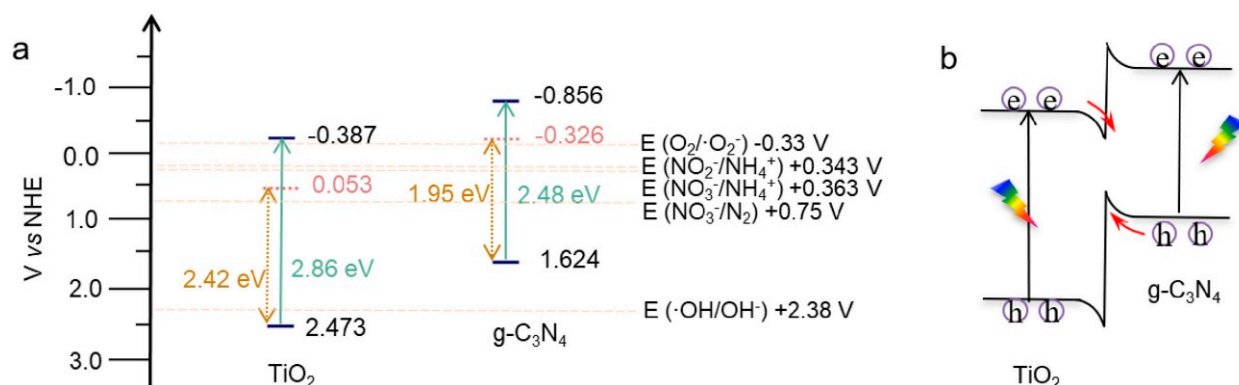


Figure 12. (a) Energy band levels of TiO_2 and $g\text{-C}_3\text{N}_4$; (b) The charge carrier transfer behavior in $g\text{-C}_3\text{N}_4/\text{RGO}/\text{TiO}_2$ material [208] (Reprinted with permission from [208] Copyright 2022 Elsevier Ltd.).

The CGTC (graphene-oxide-bridged chitin-modified TiO_2 /carbon fiber) composite prepared under hydrothermal conditions by chitin-modified and GO-bridged TiO_2 /carbon fibers showed 97% photocatalytic degradation of Rhodamine B in 60 min [208]. Yanwen et al. [209] reported the ternary composite N- TiO_2 /GO/PP fiber sheet (24.6 cm \times 2.7 cm) fabricated by the immobilization of N-doped TiO_2 and GO on polypropylene (PP). Photocatalytic degradation for 9 h under simulated sunlight of 10 mg L^{-1} roxithromycin (roxithromycin is an antibiotic pollutant from domestic and industrial effluent; its low concentrations may cause high ecological risk after long term exposure [210]) could reach up to 90%, with a degradation rate constant of 0.2299 h^{-1} in surface water under alkaline conditions (pH 8–9).

7.2. Photoconversion of CO_2

Carbon dioxide (CO_2) emission is a major source of global warming. The photoconversion of CO_2 into useful chemicals, such as CH_3OH , CH_4 , CO , etc., is an attractive approach to alleviate the issues of environmental pollution and climate change [211–214]. Kamal et al. [215] reported the synthesis of plasmonic gold nanoparticles photodeposited on TiO_2 and decorated on N-doped graphene (ANGT_x) to form a heterostructure. The composite photocatalyst showed enhanced photoconversion of CO_2 to methane with high selectivity. The optimized composite delivered the highest electron consumption rate (R_{electron}) of 742.39 $\mu\text{mol g}^{-1}\text{h}^{-1}$ in 4 h for the reduced products. The outstanding performance of such a photocatalyst was attributed to the synergistic effect between the components [215]. The improved light absorption, higher CO_2 adsorption, faster charge transfer kinetics and lower recombination rate originated from interfacial kinetics between components, and a similar enhancement was also reported for Ni/GO- TiO_2 composites [128].

7.3. Air Purification

Air pollution levels have become increasingly alarming, and outdoor and indoor air purification is becoming indispensable in different urban areas of the world. Air pollution includes organic and inorganic chemical contaminants such as volatile organic compounds (VOCs), carbon monoxide (CO), nitrogen-containing compounds (NO_x), sulfur-containing compounds (SO_x) and pathogens such as bacteria, viruses and fungi [216].

Photocatalytic air purification is the most proficient technology that facilitates the formation of reactive oxygen species (ROS) to decompose air pollutants. Photocatalytic technology offers the complete degradation of air pollutants into nontoxic final products under ambient conditions. It does not need any chemical or external energy source and operates in safe conditions [217]. The utilization of solar light under ambient conditions makes it an ideal, feasible and preferable technique [218]. TiO_2 -based photocatalysts facilitate the adsorption of environmental pollutants, owing to their favorable photocatalytic properties applicable to self-cleaning, air-purifying and antimicrobial applications [219,220]. The mixing of TiO_2 with construction materials such as cement could lower the air pollutant

concentrations [221]. TiO₂-based photocatalysts can also be applied as coatings on the interiors of buildings to improve air quality [222].

This photocatalytic approach is also effective for the inactivation of airborne microbial pathogens such as Anthrax and against the pandemic of the Coronavirus family [223,224]. Recently, an Ag/TiO₂/RGO ternary composite was also investigated as an anti-bacterial self-cleaning photocatalyst [225]. Additionally, disinfection by titania-based photocatalysts is a relatively inexpensive, non-toxic and safe method.

7.4. Water Splitting

TiO₂-based materials are considered a promising solar-light-driven photocatalyst for water splitting [40]. Edge-sulfonated graphene (RGO-SO₃H) was synthesized through a diazotization reaction coupled with TiO₂ nanoparticles to form an RGO-SO₃H/TiO₂ photocatalyst for a hydrogen evolution reaction (HER). The composite showed a hydrogen production rate of 197.1 mmol h⁻¹g⁻¹, which was higher than that for TiO₂ (5.38 times), RGO/TiO₂ (2.81 times) and SO₃H/TiO₂ (3.40 times). The improved performance of the RGO-SO₃H/TiO₂ photocatalyst is to be attributed to the synergetic effect of covalently functionalized graphene (photoelectron cocatalyst) and sulfonate ions (H⁺-adsorbed active sites) [118].

Moreover, GO sheets anchored onto Fe₂O₃-TiO₂ and V₂O₅-TiO₂ particles exhibited 398.18 and 373.01 μmol h⁻¹ HER rates under solar radiation. The enhanced HER rates were attributed to higher surface areas provided by GO, the lower recombination of photogenerated carriers and faster electron transfer rates [226]. Higher photoelectrochemical activity was also obtained for GO/In₂S₃/TiO₂ nanorods used as photocatalysts for photoelectrochemical water splitting [227]. The improved performance was attributed to the larger surface area, visible light absorption and improved carrier transport because of additional defect states [92,228–230].

Put succinctly, binary [231] and ternary [232] graphene/TiO₂-based composites offer affordable photocatalysts with feasibility in processing, responses to visible light, promising photocatalytic activity and lower recombination rates of photogenerated charge carriers. Photostability and photocatalytic performance can be enhanced by heterojunction formation and Z-scheme photocatalysts.

8. Conclusions and Future Outlook

To resolve the limitations of TiO₂ in photocatalysis, TiO₂/graphene composites are well-known and have the potential to overcome increasing energy demand and pollution remediation by means of photocatalysis. Graphene offers advantages of (i) photosensitizing TiO₂ for visible light absorption, which results in an extended range of absorption in the solar spectrum and thereby more photocatalytic activity; and (ii) cocatalysts, assisting in charge transport, prohibiting charge recombination and overcoming the sluggish charge transfer kinetics of TiO₂. Typically, the presence of graphene affects electrical conductivity and electronic features, as well as active sites (due to the good surface area of graphene sheets), and, as a result, the overall photocatalytic activity. However, surface features, the crystal structure, the extent of oxidation and the type of derivative of graphene are crucial for this. In this review, the fundamental properties of graphene and their plausible role in photocatalysis have been elaborated. The most critical aspects on how graphene and its derivatives can be identified in composites by different spectroscopic analysis techniques (such as Raman spectroscopy, FTIR spectroscopy and XPS), and what to expect with respect to their different oxidation levels, particularly at trace concentrations of graphene-based materials in a metal oxide composite, have been elaborated, with a possible "how to" guide. The current state-of-the-art applications of TiO₂/graphene composites in photocatalysis, including wastewater treatment for the removal of pollutants, air purification, water splitting for hydrogen production and the photoconversion of CO₂ into renewable fuels, have been summarized.

Despite a marked increase in the progress of these mixed composites, several questions still need to be addressed. For instance, there is no optimal method of synthesis of these mixed composites, and the same is valid for obtaining large-scale preparations of photocatalysts as well as for the synthesis of graphene with tunable and controlled degrees of oxidation. The recent progress in the design of these photocatalysts has been reviewed, and a need for an optimal and efficient fabrication method to increase the performance of graphene derivatives and their semiconductor composites stands out. In this regard, recently, a new study [10] on the direct obtaining of visible light active photocatalysts with a controlled degree of oxidation of GO has been reported. The method is new and requires further checks for large-scale implementation; however, it opens up an avenue towards the easy and green obtaining of such mixed composites, which is a step forward towards an ecofriendly design approach for GO. The mechanism of interaction of graphene derivatives with TiO₂ is still unclear or rather vague. There is a need for future efforts in order to evaluate the underlying mechanism in promoted photocatalytic activities supported by experimental and theoretical evidence as well (for instance, the positions of valence and conduction bands, the lifetime of photogenerated charge carriers, also considering the extent of graphene oxidation, etc.). The mineralization, or photocorrosion of the mixed photocatalyst also needs to be addressed. Once well-known, these aspects can lead to designs of highly efficient, reliable and very economical graphene/semiconductor composites that can then be applied in different fields of photocatalysis.

At a glance, the progress in TiO₂/graphene-based photocatalysis has been remarkable. If the limitations are addressed step by step, undoubtedly, such composites will be very useful in photocatalysis, and considerable breakthroughs can be expected in future.

Author Contributions: Conceptualization, A.N. and A.M.; methodology, A.N. and A.M.; formal analysis, A.N. and A.M.; investigation, A.M.; data curation, A.N., S.K. and A.M.; writing—original draft preparation, A.N., S.K. and A.M.; writing—review and editing, A.M.; visualization, A.N. and A.M.; supervision, A.M. and T.Y.; project administration, A.M. and T.Y. All authors have read and agreed to the published version of the manuscript.

Funding: This research received no external funding.

Conflicts of Interest: The authors declare no conflict of interest.

References

1. Purabgola, A.; Mayilswamy, N.; Kandasubramanian, B. Graphene-based TiO₂ composites for photocatalysis & environmental remediation: Synthesis and progress. *Environ. Sci. Pollut. Res.* **2022**, *29*, 32305–32325. [CrossRef]
2. Pastrana-Martínez, L.M.; Morales-Torres, S.; Figueiredo, J.L.; Faria, J.L.; Silva, A.M. Graphene photocatalysts. In *Multifunctional Photocatalytic Materials for Energy*; Woodhead Publishing: Philadelphia, PA, USA, 2018; pp. 79–101. [CrossRef]
3. Tai, X.H.; Lai, C.W.; Yang, T.C.K.; Johan, M.R.; Lee, K.M.; Chen, C.-Y.; Juan, J.C. Highly effective removal of volatile organic pollutants with p-n heterojunction photoreduced graphene oxide-TiO₂ photocatalyst. *J. Environ. Chem. Eng.* **2022**, *10*, 107304. [CrossRef]
4. Li, Z.; Yang, D.; Chu, H.; Guo, L.; Chen, T.; Mu, Y.; He, X.; Zhong, X.; Huang, B.; Zhang, S.; et al. Efficient Charge Transfer Channels in Reduced Graphene Oxide/Mesoporous TiO₂ Nanotube Heterojunction Assemblies toward Optimized Photocatalytic Hydrogen Evolution. *Nanomaterials* **2022**, *12*, 1474. [CrossRef] [PubMed]
5. Lu, K.-Q.; Li, Y.-H.; Tang, Z.-R.; Xu, Y.-J. Roles of Graphene Oxide in Heterogeneous Photocatalysis. *ACS Mater. Au* **2021**, *1*, 37–54. [CrossRef]
6. Li, X.; Yu, J.; Swelm, W.; Al-Ghamdi, A.A.; Xie, J. Graphene in Photocatalysis: A Review. *Small* **2016**, *12*, 6640–6696. [CrossRef]
7. Zhang, N.; Ning, X.; Chen, J.; Xue, J.; Lu, G.; Qiu, H. Photocatalytic degradation of tetracycline based on the highly reactive interface between graphene nanopore and TiO₂ nanoparticles. *Microporous Mesoporous Mater.* **2022**, *338*, 111958. [CrossRef]
8. Ye, X.; Zuo, S.; Wang, P.; Liu, W.; Li, X.; Yao, C. Seed-induced synthesis of durian-like mischcrystal TiO₂/graphene as an efficient photocatalyst for desulfurization. *Mol. Cryst. Liq. Cryst.* **2022**, 1–16. [CrossRef]
9. Nasir, A.; Raza, A.; Tahir, M.; Yasin, T. Free-radical graft polymerization of acrylonitrile on gamma irradiated graphene oxide: Synthesis and characterization. *Mater. Chem. Phys.* **2020**, *246*, 122807. [CrossRef]
10. Nasir, A.; Mazare, A.; Zhou, X.; Qin, S.; Denisov, N.; Zdravil, L.; Kment, Š.; Zboril, R.; Yasin, T.; Schmuki, P. Photocatalytic Synthesis of Oxidized Graphite Enabled by Grey TiO₂ and Direct Formation of a Visible-Light-Active Titania/Graphene Oxide Nanocomposite. *ChemPhotoChem* **2022**, *6*, e202100274. [CrossRef]
11. Razaq, A.; Bibi, F.; Zheng, X.; Papadakis, R.; Jafri, S.H.M.; Li, H. Review on Graphene-, Graphene Oxide-, Reduced Graphene Oxide-Based Flexible Composites: From Fabrication to Applications. *Materials* **2022**, *15*, 1012. [CrossRef]

12. Usharani, B.; Manivannan, V. Enhanced photocatalytic activity of reduced graphene oxide-TiO₂ nanocomposite for picric acid degradation. *Inorg. Chem. Commun.* **2022**, *142*, 109660. [[CrossRef](#)]
13. Humayun, M.; Wang, C.; Luo, W. Recent Progress in the Synthesis and Applications of Composite Photocatalysts: A Critical Review. *Small Methods* **2021**, *6*, 2101395. [[CrossRef](#)]
14. Schneider, J.; Matsuoka, M.; Takeuchi, M.; Zhang, J.; Horiuchi, Y.; Anpo, M.; Bahnemann, D.W. Understanding TiO₂ Photocatalysis: Mechanisms and Materials. *Chem. Rev.* **2014**, *114*, 9919–9986. [[CrossRef](#)] [[PubMed](#)]
15. Zhang, J.; Zhou, P.; Liu, J.; Yu, J. New understanding of the difference of photocatalytic activity among anatase, rutile and brookite TiO₂. *Phys. Chem. Chem. Phys.* **2014**, *16*, 20382–20386. [[CrossRef](#)] [[PubMed](#)]
16. Mattsson, A. Formic Acid Adsorption and Photodecomposition on Rutile TiO₂ (110) An In Situ Infrared Reflection Absorption Spectroscopy Study. Ph.D. Thesis, Upsala University, Uppsala, Sweden, 14 June 2014.
17. Li, C.; Gu, M.; Gao, M.; Liu, K.; Zhao, X.; Cao, N.; Feng, J.; Ren, Y.; Wei, T.; Zhang, M. N-doping TiO₂ hollow microspheres with abundant oxygen vacancies for highly photocatalytic nitrogen fixation. *J. Colloid Interface Sci.* **2021**, *609*, 341–352. [[CrossRef](#)]
18. Shoneye, A.; Chang, J.S.; Chong, M.N.; Tang, J. Recent progress in photocatalytic degradation of chlorinated phenols and reduction of heavy metal ions in water by TiO₂-based catalysts. *Int. Mater. Rev.* **2021**, *67*, 47–64. [[CrossRef](#)]
19. Zhang, J.; Lei, Y.; Cao, S.; Hu, W.; Piao, L.; Chen, X. Photocatalytic hydrogen production from seawater under full solar spectrum without sacrificial reagents using TiO₂ nanoparticles. *Nano Res.* **2021**, *15*, 2013–2022. [[CrossRef](#)]
20. Rostami, M.; Badiei, A.; Ganjali, M.R.; Rahimi-Nasrabadi, M.; Naddafi, M.; Karimi-Maleh, H. Nano-architectural design of TiO₂ for high performance photocatalytic degradation of organic pollutant: A review. *Environ. Res.* **2022**, *212*, 113347. [[CrossRef](#)]
21. Sun, Q.; Li, K.; Wu, S.; Han, B.; Sui, L.; Dong, L. Remarkable improvement of TiO₂ for dye photocatalytic degradation by a facile post-treatment. *New J. Chem.* **2020**, *44*, 1942–1952. [[CrossRef](#)]
22. Feng, T.; Feng, G.S.; Yan, L.; Pan, J.H. One-Dimensional Nanostructured TiO₂ for Photocatalytic Degradation of Organic Pollutants in Wastewater. *Int. J. Photoenergy* **2014**, *2014*, 563879. [[CrossRef](#)]
23. Rajeshwar, K.; Osugi, M.; Chanmanee, W.; Chenthamarakshan, C.; Zannoni, M.; Kajitvichyanukul, P.; Krishnan-Ayer, R. Heterogeneous photocatalytic treatment of organic dyes in air and aqueous media. *J. Photochem. Photobiol. C Photochem. Rev.* **2008**, *9*, 171–192. [[CrossRef](#)]
24. Ghaly, M.Y.; Jamil, T.S.; El-Seesy, I.E.; Souaya, E.R.; Nasr, R.A. Treatment of highly polluted paper mill wastewater by solar photocatalytic oxidation with synthesized nano TiO₂. *Chem. Eng. J.* **2011**, *168*, 446–454. [[CrossRef](#)]
25. Ajmal, A.; Majeed, I.; Malik, R.N.; Idriss, H.; Nadeem, M.A. Principles and mechanisms of photocatalytic dye degradation on TiO₂ based photocatalysts: A comparative overview. *RSC Adv.* **2014**, *4*, 37003–37026. [[CrossRef](#)]
26. Yin, J.; Zhang, X. Technologies for bHRPs and risk control. In *High-Risk Pollutants in Wastewater*; Elsevier: Amsterdam, The Netherlands, 2020; pp. 237–258. [[CrossRef](#)]
27. Pandis, P.K.; Kalogirou, C.; Kanellou, E.; Vaitsis, C.; Savvidou, M.G.; Sourkouni, G.; Zorpas, A.A.; Argiris, C. Key Points of Advanced Oxidation Processes (AOPs) for Wastewater, Organic Pollutants and Pharmaceutical Waste Treatment: A Mini Review. *ChemEngineering* **2022**, *6*, 8. [[CrossRef](#)]
28. Athanasekou, C.P.; Likodimos, V.; Falaras, P. Recent developments of TiO₂ photocatalysis involving advanced oxidation and reduction reactions in water. *J. Environ. Chem. Eng.* **2018**, *6*, 7386–7394. [[CrossRef](#)]
29. Saravanan, R.; Gracia, F.; Stephen, A. Basic Principles, Mechanism, and Challenges of Photocatalysis. In *Nanocomposites for Visible Light-Induced Photocatalysis*; Springer: Berlin/Heidelberg, Germany, 2017; pp. 19–40. [[CrossRef](#)]
30. Tismanar, I.; Obreja, A.C.; Buiu, O.; Duta, A. VIS-active TiO₂—Graphene oxide composite thin films for photocatalytic applications. *Appl. Surf. Sci.* **2020**, *538*, 147833. [[CrossRef](#)]
31. Long, Z.; Li, Q.; Wei, T.; Zhang, G.; Ren, Z. Historical development and prospects of photocatalysts for pollutant removal in water. *J. Hazard. Mater.* **2020**, *395*, 122599. [[CrossRef](#)]
32. Guo, Q.; Zhou, C.; Ma, Z.; Yang, X. Fundamentals of TiO₂ Photocatalysis: Concepts, Mechanisms, and Challenges. *Adv. Mater.* **2019**, *31*, 1901997. [[CrossRef](#)]
33. Ijaz, M.; Zafar, M. Titanium dioxide nanostructures as efficient photocatalyst: Progress, challenges and perspective. *Int. J. Energy Res.* **2020**, *45*, 3569–3589. [[CrossRef](#)]
34. Lian, P.; Qin, A.; Liao, L.; Zhang, K. Progress on the nanoscale spherical TiO₂ photocatalysts: Mechanisms, synthesis and degradation applications. *Nano Sel.* **2020**, *2*, 447–467. [[CrossRef](#)]
35. Nursam, N.; Wang, X.; Caruso, R.A. High-Throughput Synthesis and Screening of Titania-Based Photocatalysts. *ACS Comb. Sci.* **2015**, *17*, 548–569. [[CrossRef](#)]
36. Reza, K.M.; Kurny, A.S.W.; Gulshan, F. Parameters affecting the photocatalytic degradation of dyes using TiO₂: A review. *Appl. Water Sci.* **2017**, *7*, 1569–1578. [[CrossRef](#)]
37. Sun, S.; Song, P.; Cui, J.; Liang, S. Amorphous TiO₂ nanostructures: Synthesis, fundamental properties and photocatalytic applications. *Catal. Sci. Technol.* **2019**, *9*, 4198–4215. [[CrossRef](#)]
38. Djurišić, A.B.; Leung, Y.H.; Ng, A.M.C. Strategies for improving the efficiency of semiconductor metal oxide photocatalysis. *Mater. Horiz.* **2014**, *1*, 400–410. [[CrossRef](#)]
39. Luo, J.; Zhang, S.; Sun, M.; Yang, L.; Luo, S.; Crittenden, J.C. A Critical Review on Energy Conversion and Environmental Remediation of Photocatalysts with Remodeling Crystal Lattice, Surface, and Interface. *ACS Nano* **2019**, *13*, 9811–9840. [[CrossRef](#)]

40. Miyoshi, A.; Nishioka, S.; Maeda, K. Water Splitting on Rutile TiO₂-Based Photocatalysts. *Chem. Eur. J.* **2018**, *24*, 18204–18219. [[CrossRef](#)] [[PubMed](#)]
41. Deng, Q.; Zhang, W.; Lan, T.; Xie, J.; Xie, W.; Liu, Z.; Huang, Y.; Wei, M. Anatase TiO₂ Quantum Dots with a Narrow Band Gap of 2.85 eV Based on Surface Hydroxyl Groups Exhibiting Significant Photodegradation Property. *Eur. J. Inorg. Chem.* **2018**, *2018*, 1506–1510. [[CrossRef](#)]
42. Parangi, T.; Mishra, M.K. Titania Nanoparticles as Modified Photocatalysts: A Review on Design and Development. *Comments Inorg. Chem.* **2019**, *39*, 90–126. [[CrossRef](#)]
43. Paramasivam, I.; Jha, H.; Liu, N.; Schmuki, P. A Review of Photocatalysis using Self-organized TiO₂ Nanotubes and Other Ordered Oxide Nanostructures. *Small* **2012**, *8*, 3073–3103. [[CrossRef](#)]
44. Gupta, T.; Samriti; Cho, J.; Prakash, J. Hydrothermal synthesis of TiO₂ nanorods: Formation chemistry, growth mechanism, and tailoring of surface properties for photocatalytic activities. *Mater. Today Chem.* **2021**, *20*, 100428. [[CrossRef](#)]
45. Edy, R.; Zhao, Y.; Huang, G.S.; Shi, J.J.; Zhang, J.; Solovev, A.A.; Mei, Y. TiO₂ nanosheets synthesized by atomic layer deposition for photocatalysis. *Prog. Nat. Sci.* **2016**, *26*, 493–497. [[CrossRef](#)]
46. Li, S.; Xiong, J.; Lu, M.; Li, W.; Cheng, G. Fabrication Approach Impact on Solar-to-Hydrogen Evolution of Protonic Titanate-Derived Nano-TiO₂. *Ind. Eng. Chem. Res.* **2022**, *61*, 11347–11356. [[CrossRef](#)]
47. Lyu, Y.; Asoh, T.-A.; Uyama, H. Hierarchically porous TiO₂ monolith prepared using a cellulose monolith as a template. *Mater. Chem. Front.* **2021**, *5*, 3877–3885. [[CrossRef](#)]
48. Verma, R.; Gangwar, J.; Srivastava, A.K. Multiphase TiO₂ nanostructures: A review of efficient synthesis, growth mechanism, probing capabilities, and applications in bio-safety and health. *RSC Adv.* **2017**, *7*, 44199–44224. [[CrossRef](#)]
49. Hu, W.; Li, L.; Li, G.; Liu, Y.; Withers, R. Atomic-scale control of TiO₆ octahedra through solution chemistry towards giant dielectric response. *Sci. Rep.* **2014**, *4*, 6582. [[CrossRef](#)] [[PubMed](#)]
50. Kapilashrami, M.; Zhang, Y.; Liu, Y.-S.; Hagfeldt, A.; Guo, J. Probing the Optical Property and Electronic Structure of TiO₂ Nanomaterials for Renewable Energy Applications. *Chem. Rev.* **2014**, *114*, 9662–9707. [[CrossRef](#)]
51. Luttrell, T.; Halpegamage, S.; Tao, J.; Kramer, A.; Sutter, E.; Batzill, M. Why is anatase a better photocatalyst than rutile?—Model studies on epitaxial TiO₂ films. *Sci. Rep.* **2014**, *4*, 4043. [[CrossRef](#)]
52. De Angelis, F.; Di Valentin, C.; Fantacci, S.; Vittadini, A.; Selloni, A. Theoretical Studies on Anatase and Less Common TiO₂ Phases: Bulk, Surfaces, and Nanomaterials. *Chem. Rev.* **2014**, *114*, 9708–9753. [[CrossRef](#)]
53. Wen, J.; Li, X.; Liu, W.; Fang, Y.; Xie, J.; Xu, Y. Photocatalysis fundamentals and surface modification of TiO₂ nanomaterials. *Chin. J. Catal.* **2015**, *36*, 2049–2070. [[CrossRef](#)]
54. Nah, Y.-C.; Paramasivam, I.; Schmuki, P. Doped TiO₂ and TiO₂ Nanotubes: Synthesis and Applications. *ChemPhysChem* **2010**, *11*, 2698–2713. [[CrossRef](#)]
55. Ji, L.; Zhou, X.; Schmuki, P. Sulfur and Ti³⁺ co-Doping of TiO₂ Nanotubes Enhance Photocatalytic H₂ Evolution without the Use of Any co-catalyst. *Chem. Asian J.* **2019**, *14*, 2724–2730. [[CrossRef](#)] [[PubMed](#)]
56. Naldoni, A.; Altomare, M.; Zoppellaro, G.; Liu, N.; Kment, Š.; Zboril, R.; Schmuki, P. Photocatalysis with Reduced TiO₂: From Black TiO₂ to Cocatalyst-Free Hydrogen Production. *ACS Catal.* **2018**, *9*, 345–364. [[CrossRef](#)]
57. Mohajernia, S.; Andryskova, P.; Zoppellaro, G.; Hejazi, S.; Kment, S.; Zboril, R.; Schmidt, J.; Schmuki, P. Influence of Ti³⁺ defect-type on heterogeneous photocatalytic H₂ evolution activity of TiO₂. *J. Mater. Chem. A* **2019**, *8*, 1432–1442. [[CrossRef](#)]
58. Zhou, X.; Liu, N.; Schmuki, P. Photocatalysis with TiO₂ Nanotubes: “Colorful” Reactivity and Designing Site-Specific Photocatalytic Centers into TiO₂ Nanotubes. *ACS Catal.* **2017**, *7*, 3210–3235. [[CrossRef](#)]
59. Gao, Z.-D.; Qu, Y.-F.; Zhou, X.; Wang, L.; Song, Y.-Y.; Schmuki, P. Pt-Decorated g-C₃N₄ /TiO₂ Nanotube Arrays with Enhanced Visible-Light Photocatalytic Activity for H₂ Evolution. *ChemistryOpen* **2016**, *5*, 197–200. [[CrossRef](#)] [[PubMed](#)]
60. Etacheri, V.; Di Valentin, C.; Schneider, J.; Bahnemann, D.; Pillai, S.C. Visible-light activation of TiO₂ photocatalysts: Advances in theory and experiments. *J. Photochem. Photobiol. C Photochem. Rev.* **2015**, *25*, 1–29. [[CrossRef](#)]
61. Mittal, A.; Mari, B.; Sharma, S.; Kumari, V.; Maken, S.; Kumari, K.; Kumar, N. Non-metal modified TiO₂: A step towards visible light photocatalysis. *J. Mater. Sci. Mater. Electron.* **2019**, *30*, 3186–3207. [[CrossRef](#)]
62. Kaur, N.; Shahi, S.K.; Shahi, J.; Sandhu, S.; Sharma, R.; Singh, V. Comprehensive review and future perspectives of efficient N-doped, Fe-doped and (N,Fe)-co-doped titania as visible light active photocatalysts. *Vacuum* **2020**, *178*, 109429. [[CrossRef](#)]
63. Ismael, M. A review and recent advances in solar-to-hydrogen energy conversion based on photocatalytic water splitting over doped-TiO₂ nanoparticles. *Sol. Energy* **2020**, *211*, 522–546. [[CrossRef](#)]
64. Paumo, H.K.; Dalhatou, S.; Katata-Seru, L.M.; Kamdem, B.P.; Tijani, J.O.; Vishwanathan, V.; Kane, A.; Bahadur, I. TiO₂ assisted photocatalysts for degradation of emerging organic pollutants in water and wastewater. *J. Mol. Liq.* **2021**, *331*, 115458. [[CrossRef](#)]
65. Arora, I.; Chawla, H.; Chandra, A.; Sagadevan, S.; Garg, S. Advances in the strategies for enhancing the photocatalytic activity of TiO₂: Conversion from UV-light active to visible-light active photocatalyst. *Inorg. Chem. Commun.* **2022**, *143*, 109700. [[CrossRef](#)]
66. Wang, Y.; Li, L.; Lu, H.; Wang, C.; Zhao, Y.; Kuga, S.; Huang, Y.; Wu, M. Effect of morphology-induced interfacial defects on band location and enhanced photocatalytic dye degradation activity of TiO₂/Graphene aerogel. *J. Phys. Chem. Solids* **2021**, *162*, 110448. [[CrossRef](#)]
67. Cheng, L.; Xiang, Q.; Liao, Y.; Zhang, H. CdS-Based Photocatalysts. *Energy Environ. Sci.* **2018**, *11*, 1362–1391. [[CrossRef](#)]
68. Noor, M.; Sharmin, F.; Al Mamun, M.; Hasan, S.; Hakim, M.; Basith, M. Effect of Gd and Y co-doping in BiVO₄ photocatalyst for enhanced degradation of methylene blue dye. *J. Alloy. Compd.* **2021**, *895*, 162639. [[CrossRef](#)]

69. Singh, S.; Modak, A.; Pant, K.K.; Sinhamahapatra, A.; Biswas, P. MoS₂-Nanosheets-Based Catalysts for Photocatalytic CO₂ Reduction: A Review. *ACS Appl. Nano Mater.* **2021**, *4*, 8644–8667. [\[CrossRef\]](#)
70. Xiang, Q.; Yu, J.; Jaroniec, M. Graphene-based semiconductor photocatalysts. *Chem. Soc. Rev.* **2012**, *41*, 782–796. [\[CrossRef\]](#)
71. Yu, Y.-J.; Zhao, Y.; Ryu, S.; Brus, L.E.; Kim, K.S.; Kim, P. Tuning the Graphene Work Function by Electric Field Effect. *Nano Lett.* **2009**, *9*, 3430–3434. [\[CrossRef\]](#)
72. Kim, J.-H.; Hwang, J.H.; Suh, J.; Tongay, S.; Kwon, S.; Hwang, C.C.; Wu, J.; Park, J.Y. Work function engineering of single layer graphene by irradiation-induced defects. *Appl. Phys. Lett.* **2013**, *103*, 171604. [\[CrossRef\]](#)
73. Akada, K.; Terasawa, T.-O.; Imamura, G.; Obata, S.; Saiki, K. Control of work function of graphene by plasma assisted nitrogen doping. *Appl. Phys. Lett.* **2014**, *104*, 131602. [\[CrossRef\]](#)
74. Kwon, K.C.; Choi, K.S.; Kim, C.; Kim, S.Y. Role of Metal Cations in Alkali Metal Chloride Doped Graphene. *J. Phys. Chem. C* **2014**, *118*, 8187–8193. [\[CrossRef\]](#)
75. Jung, I.; Dikin, D.A.; Piner, R.D.; Ruoff, R.S. Tunable Electrical Conductivity of Individual Graphene Oxide Sheets Reduced at “Low” Temperatures. *Nano Lett.* **2008**, *8*, 4283–4287. [\[CrossRef\]](#) [\[PubMed\]](#)
76. Eda, G.; Mattevi, C.; Yamaguchi, H.; Kim, H.; Chhowalla, M. Insulator to Semimetal Transition in Graphene Oxide. *J. Phys. Chem. C* **2009**, *113*, 15768–15771. [\[CrossRef\]](#)
77. Jung, I.; Pelton, M.; Piner, R.; Dikin, D.A.; Stankovich, S.; Watcharotone, S.; Hausner, A.M.; Ruoff, R.S. Simple Approach for High-Contrast Optical Imaging and Characterization of Graphene-Based Sheets. *Nano Lett.* **2007**, *7*, 3569–3575. [\[CrossRef\]](#)
78. Jung, I.; Vaupel, M.; Pelton, M.; Piner, R.; Dikin, D.A.; Stankovich, S.; An, J.; Ruoff, R.S. Characterization of Thermally Reduced Graphene Oxide by Imaging Ellipsometry. *J. Phys. Chem. C* **2008**, *112*, 8499–8506. [\[CrossRef\]](#)
79. Trapalis, A.; Todorova, N.; Giannakopoulou, T.; Boukos, N.; Speliotis, T.; Dimotikali, D.; Yu, J. TiO₂/graphene composite photocatalysts for NO_x removal: A comparison of surfactant-stabilized graphene and reduced graphene oxide. *Appl. Catal. B Environ.* **2016**, *180*, 637–647. [\[CrossRef\]](#)
80. Mallick, B.C.; Hsieh, C.-T.; Yin, K.-M.; Li, J.; Gandomi, Y.A. Linear control of the oxidation level on graphene oxide sheets using the cyclic atomic layer reduction technique. *Nanoscale* **2019**, *11*, 7833–7838. [\[CrossRef\]](#) [\[PubMed\]](#)
81. Wu, R.; Wang, Y.; Chen, L.; Huang, L.; Chen, Y. Control of the oxidation level of graphene oxide for high efficiency polymer solar cells. *RSC Adv.* **2015**, *5*, 49182–49187. [\[CrossRef\]](#)
82. Kholmanov, I.N.; Magnuson, C.W.; Aliev, A.E.; Li, H.; Zhang, B.; Suk, J.W.; Zhang, L.L.; Peng, E.; Mousavi, S.H.; Khanikaev, A.B.; et al. Improved Electrical Conductivity of Graphene Films Integrated with Metal Nanowires. *Nano Lett.* **2012**, *12*, 5679–5683. [\[CrossRef\]](#)
83. Si, Y.; Samulski, E.T. Synthesis of water soluble graphene. *Nano Lett.* **2008**, *8*, 1679–1682. [\[CrossRef\]](#)
84. Jaafar, E.; Kashif, M.; Sahari, S.; Ngaini, Z. Study on Morphological, Optical and Electrical Properties of Graphene Oxide (GO) and Reduced Graphene Oxide (rGO). *Mater. Sci. Forum* **2018**, *917*, 112–116. [\[CrossRef\]](#)
85. Pham, V.H.; Pham, H.D.; Dang, T.T.; Hur, S.H.; Kim, E.J.; Kong, B.S.; Kim, S.; Chung, J.S. Chemical reduction of an aqueous suspension of graphene oxide by nascent hydrogen. *J. Mater. Chem.* **2012**, *22*, 10530–10536. [\[CrossRef\]](#)
86. Stankovich, S.; Dikin, D.A.; Piner, R.D.; Kohlhaas, K.A.; Kleinhammes, A.; Jia, Y.; Wu, Y.; Nguyen, S.T.; Ruoff, R.S. Synthesis of graphene-based nanosheets via chemical reduction of exfoliated graphite oxide. *Carbon* **2007**, *45*, 1558–1565. [\[CrossRef\]](#)
87. Moon, I.K.; Lee, J.; Ruoff, R.S.; Lee, H. Reduced graphene oxide by chemical graphitization. *Nat. Commun.* **2010**, *1*, 73. [\[CrossRef\]](#) [\[PubMed\]](#)
88. Husnah, M.; A Fakhri, H.; Rohman, F.; Aimon, A.H.; Iskandar, F. A modified Marcano method for improving electrical properties of reduced graphene oxide (rGO). *Mater. Res. Express* **2017**, *4*, 064001. [\[CrossRef\]](#)
89. Loh, K.P.; Bao, Q.; Eda, G.; Chhowalla, M. Graphene oxide as a chemically tunable platform for optical applications. *Nat. Chem.* **2010**, *2*, 1015–1024. [\[CrossRef\]](#) [\[PubMed\]](#)
90. Ogino, I.; Fukazawa, G.; Kamatari, S.; Iwamura, S.; Mukai, S.R. The critical role of bulk density of graphene oxide in tuning its defect concentration through microwave-driven annealing. *J. Energy Chem.* **2018**, *27*, 1468–1474. [\[CrossRef\]](#)
91. Zhang, H.; Huang, M.; Song, J.; Sun, D.; Qiao, Y.; Zhou, X.; Ye, C.; Liu, W.; Wei, Z.; Peng, G.; et al. Effect of the defect densities of reduced graphene oxide network on the stability of lithium-metal anodes. *Mater. Today Commun.* **2021**, *27*, 102276. [\[CrossRef\]](#)
92. Moustafa, H.M.; Mahmoud, M.S.; Nassar, M.M. Photon-induced water splitting experimental and kinetic studies with a hydrothermally prepared TiO₂-doped rGO photocatalyst. *Inorg. Chem. Commun.* **2022**, *141*, 109546. [\[CrossRef\]](#)
93. Zhang, S.; Wang, H.; Liu, J.; Bao, C. Measuring the specific surface area of monolayer graphene oxide in water. *Mater. Lett.* **2020**, *261*, 127098. [\[CrossRef\]](#)
94. Esmaeili, A.; Entezari, M. Facile and fast synthesis of graphene oxide nanosheets via bath ultrasonic irradiation. *J. Colloid Interface Sci.* **2014**, *432*, 19–25. [\[CrossRef\]](#)
95. Huang, X.; Qi, X.; Boey, F.; Zhang, H. Graphene-based composites. *Chem. Soc. Rev.* **2012**, *41*, 666–686. [\[CrossRef\]](#) [\[PubMed\]](#)
96. Xiang, Q.; Cheng, B.; Yu, J. Graphene-Based Photocatalysts for Solar-Fuel Generation. *Angew. Chem. Int. Ed.* **2015**, *54*, 11350–11366. [\[CrossRef\]](#)
97. Yeh, T.-F.; Syu, J.-M.; Cheng, C.; Chang, T.-H.; Teng, H. Graphite Oxide as a Photocatalyst for Hydrogen Production from Water. *Adv. Funct. Mater.* **2010**, *20*, 2255–2262. [\[CrossRef\]](#)

98. Raghavan, A.; Sarkar, S.; Nagappagari, L.R.; Bojja, S.; Muthukondavenkatakrishnan, S.; Ghosh, S. Decoration of Graphene Quantum Dots on TiO₂ Nanostructures: Photosensitizer and Cocatalyst Role for Enhanced Hydrogen Generation. *Ind. Eng. Chem. Res.* **2020**, *59*, 13060–13068. [[CrossRef](#)]
99. Zeng, P.; Zhang, Q.; Zhang, X.; Peng, T. Graphite oxide—TiO₂ nanocomposite and its efficient visible-light-driven photocatalytic hydrogen production. *J. Alloy. Compd.* **2012**, *516*, 85–90. [[CrossRef](#)]
100. Yeh, T.-F.; Chan, F.-F.; Hsieh, C.-T.; Teng, H. Graphite Oxide with Different Oxygenated Levels for Hydrogen and Oxygen Production from Water under Illumination: The Band Positions of Graphite Oxide. *J. Phys. Chem. C* **2011**, *115*, 22587–22597. [[CrossRef](#)]
101. Moon, G.-H.; Kim, D.-H.; Kim, H.-I.; Bokare, A.D.; Choi, W. Platinum-like Behavior of Reduced Graphene Oxide as a Cocatalyst on TiO₂ for the Efficient Photocatalytic Oxidation of Arsenite. *Environ. Sci. Technol. Lett.* **2014**, *1*, 185–190. [[CrossRef](#)]
102. Kusiak-Nejman, E.; Morawski, A.W. TiO₂/graphene-based nanocomposites for water treatment: A brief overview of charge carrier transfer, antimicrobial and photocatalytic performance. *Appl. Catal. B Environ.* **2019**, *253*, 179–186. [[CrossRef](#)]
103. Yang, M.-Q.; Xu, Y.-J. Basic Principles for Observing the Photosensitizer Role of Graphene in the Graphene–Semiconductor Composite Photocatalyst from a Case Study on Graphene–ZnO. *J. Phys. Chem. C* **2013**, *117*, 21724–21734. [[CrossRef](#)]
104. Du, A.; Ng, Y.H.; Bell, N.J.; Zhu, Z.; Amal, R.; Smith, S.C. Hybrid Graphene/Titania Nanocomposite: Interface Charge Transfer, Hole Doping, and Sensitization for Visible Light Response. *J. Phys. Chem. Lett.* **2011**, *2*, 894–899. [[CrossRef](#)]
105. Morales-Torres, S.; Pastrana-Martinez, L.M.; Figueiredo, J.L.; Faria, J.L.; Silva, A.M. Design of graphene-based TiO₂ photocatalysts—A review. *Environ. Sci. Pollut. Res.* **2012**, *19*, 3676–3687. [[CrossRef](#)] [[PubMed](#)]
106. Yadav, H.M.; Kim, J.-S. Solvothermal synthesis of anatase TiO₂-graphene oxide nanocomposites and their photocatalytic performance. *J. Alloy. Compd.* **2016**, *688*, 123–129. [[CrossRef](#)]
107. Guo, J.; Zhu, S.; Chen, Z.; Li, Y.; Yu, Z.; Liu, Q.; Li, J.; Feng, C.; Zhang, D. Sonochemical synthesis of TiO₂ nanoparticles on graphene for use as photocatalyst. *Ultrason. Sonochem.* **2011**, *18*, 1082–1090. [[CrossRef](#)] [[PubMed](#)]
108. Bell, N.J.; Ng, Y.H.; Du, A.; Coster, H.; Smith, S.C.; Amal, R. Understanding the Enhancement in Photoelectrochemical Properties of Photocatalytically Prepared TiO₂-Reduced Graphene Oxide Composite. *J. Phys. Chem. C* **2011**, *115*, 6004–6009. [[CrossRef](#)]
109. Bhanvase, B.A.; Shende, T.P.; Sonawane, S.H. A review on graphene–TiO₂ and doped graphene–TiO₂ nanocomposite photocatalyst for water and wastewater treatment. *Environ. Technol. Rev.* **2017**, *6*, 1–14. [[CrossRef](#)]
110. Liang, Y.; Wang, H.; Casalongue, H.S.; Chen, Z.; Dai, H. TiO₂ nanocrystals grown on graphene as advanced photocatalytic hybrid materials. *Nano Res.* **2010**, *3*, 701–705. [[CrossRef](#)]
111. Wang, J.; Wang, P.; Cao, Y.; Chen, J.; Li, W.; Shao, Y.; Zheng, Y.; Li, D. A high efficient photocatalyst Ag₃VO₄/TiO₂/graphene nanocomposite with wide spectral response. *Appl. Catal. B Environ.* **2013**, *136–137*, 94–102. [[CrossRef](#)]
112. Huang, Q.; Tian, S.; Zeng, D.; Wang, X.; Song, W.; Li, Y.; Xiao, W.; Xie, C. Enhanced Photocatalytic Activity of Chemically Bonded TiO₂/Graphene Composites Based on the Effective Interfacial Charge Transfer through the C–Ti Bond. *ACS Catal.* **2013**, *3*, 1477–1485. [[CrossRef](#)]
113. Chen, C.; Cai, W.; Long, M.; Zhou, B.; Wu, Y.; Wu, D.; Feng, Y. Synthesis of Visible-Light Responsive Graphene Oxide/TiO₂ Composites with p/n Heterojunction. *ACS Nano* **2010**, *4*, 6425–6432. [[CrossRef](#)]
114. Rotami, M.; Hamadianian, M.; Rahimi-Nasrabadi, M.; Ganjali, M.R. Sol-gel preparation of metal and nonmetal-codoped TiO₂-graphene nanophotocatalyst for photodegradation of MO under UV and visible-light irradiation. *Ionics* **2019**, *25*, 1869–1878. [[CrossRef](#)]
115. Liu, C.; Teng, Y.; Liu, R.; Luo, S.; Tang, Y.; Chen, L.; Cai, Q. Fabrication of graphene films on TiO₂ nanotube arrays for photocatalytic application. *Carbon* **2011**, *49*, 5312–5320. [[CrossRef](#)]
116. Zubair, M.; Kim, H.; Razaq, A.; Grimes, C.A.; In, S.-I. Solar spectrum photocatalytic conversion of CO₂ to CH₄ utilizing TiO₂ nanotube arrays embedded with graphene quantum dots. *J. CO₂ Util.* **2018**, *26*, 70–79. [[CrossRef](#)]
117. Wang, G.; Zhang, Q.; Chen, Q.; Ma, X.; Xin, Y.; Zhu, X.; Ma, D.; Cui, C.; Zhang, J.; Xiao, Z. Photocatalytic degradation performance and mechanism of dibutyl phthalate by graphene/TiO₂ nanotube array photoelectrodes. *Chem. Eng. J.* **2018**, *358*, 1083–1090. [[CrossRef](#)]
118. Wang, P.; Deng, P.; Cao, Y. Edge-sulfonated graphene-decorated TiO₂ photocatalyst with high H₂-evolution performance. *Int. J. Hydrog. Energy* **2021**, *47*, 1006–1015. [[CrossRef](#)]
119. Wang, Z. Electrochemical Study and Synthesis of Highly-ordered TiO₂ Nanorods Arrays on 3D Graphene Oxide Framework as Photocatalyst for Acid Orange 7 Degradation. *Int. J. Electrochem. Sci.* **2022**. [[CrossRef](#)]
120. Trinh, T.T.P.N.X.; Giang, N.T.H.; Huong, L.M.; Thinh, D.B.; Dat, N.M.; Trinh, D.N.; Hai, N.D.; Oanh, D.T.Y.; Nam, H.M.; Phong, M.T.; et al. Hydrothermal synthesis of titanium dioxide/graphene aerogel for photodegradation of methylene blue in aqueous solution. *J. Sci. Adv. Mater. Devices* **2022**, *7*, 100433. [[CrossRef](#)]
121. Winayu, B.N.R.; Mao, W.-H.; Chu, H. Combination of rGO/S, N/TiO₂ for the enhancement of visible light-driven toluene photocatalytic degradation. *Sustain. Environ. Res.* **2022**, *32*, 34. [[CrossRef](#)]
122. İlhan, H.; Cayci, G.B.D.; Aksoy, E.; Diker, H.; Varlikli, C. Photocatalytic activity of dye-sensitized and non-sensitized GO-TiO₂ nanocomposites under simulated and direct sunlight. *Int. J. Appl. Ceram. Technol.* **2022**, *19*, 425–435. [[CrossRef](#)]
123. Manojkumar, P.; Lokeshkumar, E.; Premchand, C.; Saikiran, A.; Krishna, L.R.; Rameshbabu, N. Facile preparation of immobilised visible light active W-TiO₂/rGO composite photocatalyst by plasma electrolytic oxidation process. *Phys. B Condens. Matter* **2022**, *631*, 413680. [[CrossRef](#)]

124. Devi, A.D.; Pushpavanam, S.; Singh, N.; Verma, J.; Kaur, M.P.; Roy, S.C. Enhanced methane yield by photoreduction of CO₂ at moderate temperature and pressure using Pt coated, graphene oxide wrapped TiO₂ nanotubes. *Results Eng.* **2022**, *14*, 100441. [[CrossRef](#)]
125. Rawal, J.; Kamran, U.; Park, M.; Pant, B.; Park, S.-J. Nitrogen and Sulfur Co-Doped Graphene Quantum Dots Anchored TiO₂ Nanocomposites for Enhanced Photocatalytic Activity. *Catalysts* **2022**, *12*, 548. [[CrossRef](#)]
126. Li, Z.; Liu, Z.; Yang, X.; Chen, A.; Chen, P.; Yang, L.; Yan, C.; Shi, Y. Enhanced Photocatalysis of Black TiO₂/Graphene Composites Synthesized by a Facile Sol–Gel Method Combined with Hydrogenation Process. *Materials* **2022**, *15*, 3336. [[CrossRef](#)] [[PubMed](#)]
127. Jiang, M.; Zhang, M.; Wang, L.; Fei, Y.; Wang, S.; Núñez-Delgado, A.; Bokhari, A.; Race, M.; Khataee, A.; Klemeš, J.J.; et al. Photocatalytic degradation of xanthate in flotation plant tailings by TiO₂/graphene nanocomposites. *Chem. Eng. J.* **2021**, *431*, 134104. [[CrossRef](#)]
128. Quiroz-Cardoso, O.; Suárez, V.; Oros-Ruiz, S.; Quintana, M.; Ramírez-Rave, S.; Suárez-Quezada, M.; Gómez, R. Synthesis of Ni/GO-TiO₂ composites for the photocatalytic hydrogen production and CO₂ reduction to methanol. *Top. Catal.* **2022**, *2022*, 1–13. [[CrossRef](#)]
129. Kisielevska, A.; Spilarewicz-Stanek, K.; Cichomski, M.; Kozłowski, W.; Piwoński, I. The role of graphene oxide and its reduced form in the in situ photocatalytic growth of silver nanoparticles on graphene-TiO₂ nanocomposites. *Appl. Surf. Sci.* **2021**, *576*, 151759. [[CrossRef](#)]
130. Cai, D.; Tao, E.; Yang, S.; Ma, Z.; Li, Y.; Liu, L.; Wang, D.; Qian, J. Effect of mixed-phase TiO₂ doped with Ca²⁺ on charge transfer at the TiO₂/graphene interface. *Electrochim. Acta* **2022**, *422*, 140503. [[CrossRef](#)]
131. González, V.J.; Vázquez, E.; Villajos, B.; Tolosana-Moranchel, A.; Duran-Valle, C.; Faraldos, M.; Bahamonde, A. Eco-friendly mechanochemical synthesis of titania-graphene nanocomposites for pesticide photodegradation. *Sep. Purif. Technol.* **2022**, *289*, 120638. [[CrossRef](#)]
132. Khavar, A.H.C.; Khazaei, Z.; Mahjoub, A.R.; Nejat, R. TiO₂ supported-reduced graphene oxide co-doped with gallium and sulfur as an efficient heterogeneous catalyst for the selective photochemical oxidation of alcohols; DFT and mechanism insights. *J. Photochem. Photobiol. A Chem.* **2022**, *431*, 114020. [[CrossRef](#)]
133. Wu, J.-B.; Lin, M.-L.; Cong, X.; Liu, H.-N.; Tan, P.-H. Raman spectroscopy of graphene-based materials and its applications in related devices. *Chem. Soc. Rev.* **2018**, *47*, 1822–1873. [[CrossRef](#)]
134. Lee, A.Y.; Yang, K.; Anh, N.D.; Park, C.; Lee, S.M.; Lee, T.G.; Jeong, M.S. Raman study of D* band in graphene oxide and its correlation with reduction. *Appl. Surf. Sci.* **2020**, *536*, 147990. [[CrossRef](#)]
135. Qi, P.; Wang, J.; Djitcheu, X.; He, D.; Liu, H.; Zhang, Q. Techniques for the characterization of single atom catalysts. *RSC Adv.* **2021**, *12*, 1216–1227. [[CrossRef](#)] [[PubMed](#)]
136. Greczynski, G.; Hultman, L. The same chemical state of carbon gives rise to two peaks in X-ray photoelectron spectroscopy. *Sci. Rep.* **2021**, *11*, 11195. [[CrossRef](#)] [[PubMed](#)]
137. Ebnesajjad, S. Surface and Material Characterization Techniques. In *Surface Treatment of Materials for Adhesive Bonding*, 2nd ed.; Elsevier: Amsterdam, The Netherlands, 2014; pp. 39–75. [[CrossRef](#)]
138. Shahrezaei, M.; Hejazi, S.M.H.; Rambabu, Y.; Vavrecka, M.; Bakandritsos, A.; Oezkan, S.; Zboril, R.; Schmuki, P.; Naldoni, A.; Kment, S. Multi-Leg TiO₂ Nanotube Photoelectrodes Modified by Platinized Cyanographene with Enhanced Photoelectrochemical Performance. *Catalysts* **2020**, *10*, 717. [[CrossRef](#)]
139. Ferrari, A.C. Raman spectroscopy of graphene and graphite: Disorder, electron–phonon coupling, doping and nonadiabatic effects. *Solid State Commun.* **2007**, *143*, 47–57. [[CrossRef](#)]
140. Sa-Ard, W.C.; Fawcett, D.; Fung, C.C.; Chapman, P.; Rattan, S.; Poinern, G.E.J. Synthesis, characterisation and thermo-physical properties of highly stable graphene oxide-based aqueous nanofluids for potential low-temperature direct absorption solar applications. *Sci. Rep.* **2021**, *11*, 16549. [[CrossRef](#)]
141. Kudin, K.N.; Ozbas, B.; Schniepp, H.C.; Prud'homme, R.K.; Aksay, I.A.; Car, R. Raman Spectra of Graphite Oxide and Functionalized Graphene Sheets. *Nano Lett.* **2007**, *8*, 36–41. [[CrossRef](#)]
142. Kaniyoor, A.; Ramaprabhu, S. A Raman spectroscopic investigation of graphite oxide derived graphene. *AIP Adv.* **2012**, *2*, 032183. [[CrossRef](#)]
143. Liu, H.; Chen, Z.; Zhang, L.; Zhu, D.; Zhang, Q.; Luo, Y.; Shao, X. Graphene Grown on Anatase–TiO₂ Nanosheets: Enhanced Photocatalytic Activity on Basis of a Well-Controlled Interface. *J. Phys. Chem. C* **2018**, *122*, 6388–6396. [[CrossRef](#)]
144. Younis, U.; Rahi, A.A.; Danish, S.; Ali, M.A.; Ahmed, N.; Datta, R.; Fahad, S.; Holatko, J.; Hammerschmidt, T.; Brtnicky, M.; et al. Fourier Transform Infrared Spectroscopy vibrational bands study of *Spinacia oleracea* and *Trigonella corniculata* under biochar amendment in naturally contaminated soil. *PLoS ONE* **2021**, *16*, e0253390. [[CrossRef](#)]
145. Fahlhelbom, K.M.; Saleh, A.; Al-Tabakha, M.M.A.; Ashames, A.A. Recent applications of quantitative analytical FTIR spectroscopy in pharmaceutical, biomedical, and clinical fields: A brief review. *Rev. Anal. Chem.* **2022**, *41*, 21–33. [[CrossRef](#)]
146. Țucureanu, V.; Matei, A.; Avram, A.M. FTIR Spectroscopy for Carbon Family Study. *Crit. Rev. Anal. Chem.* **2016**, *46*, 502–520. [[CrossRef](#)] [[PubMed](#)]
147. Wang, S.; Zhu, J.; Rao, Y.; Li, B.; Zhao, S.; Bai, H.; Cui, J. Polydopamine Modified Graphene Oxide-TiO₂ Nanofiller for Reinforcing Physical Properties and Anticorrosion Performance of Waterborne Epoxy Coatings. *Appl. Sci.* **2019**, *9*, 3760. [[CrossRef](#)]

148. Zhang, H.; Wang, X.; Li, N.; Xia, J.; Meng, Q.; Ding, J.; Lu, J. Synthesis and characterization of TiO₂/graphene oxide nanocomposites for photoreduction of heavy metal ions in reverse osmosis concentrate. *RSC Adv.* **2018**, *8*, 34241–34251. [[CrossRef](#)] [[PubMed](#)]
149. Chougala, L.S.; Yatnatti, M.S.; Linganagoudar, R.K.; Kamble, R.R.; Kadadevarmath, J.S. A Simple Approach on Synthesis of TiO₂ Nanoparticles and its Application in dye Sensitized Solar Cells. *J. Nano-Electron. Phys.* **2017**, *9*, 04005-1–04005-6. [[CrossRef](#)]
150. Kocijan, M.; Ćurković, L.; Ljubas, D.; Mužina, K.; Bačić, I.; Radošević, T.; Podlogar, M.; Bdikin, I.; Otero-Irurueta, G.; Hortigüela, M.J.; et al. Graphene-based TiO₂ nanocomposite for photocatalytic degradation of dyes in aqueous solution under solar-like radiation. *Appl. Sci.* **2021**, *11*, 3966. [[CrossRef](#)]
151. Gong, Y.; Ma, X.; Dang, R.; Liu, J.; Cao, J. Synthesis of highly dispersed and versatile anatase TiO₂ nanocrystals on graphene sheets with enhanced photocatalytic performance for dye degradation. *J. Mater. Sci. Mater. Electron.* **2017**, *28*, 18883–18890. [[CrossRef](#)]
152. Sim, L.C.; Leong, K.H.; Ibrahim, S.; Saravanan, P. Graphene oxide and Ag engulfed TiO₂ nanotube arrays for enhanced electron mobility and visible-light-driven photocatalytic performance. *J. Mater. Chem. A* **2014**, *2*, 5315–5322. [[CrossRef](#)]
153. Bulusheva, L.G.; Kanygin, M.A.; Arkhipov, V.E.; Popov, K.M.; Fedoseeva, Y.V.; Smirnov, D.A.; Okotrub, A.V. In Situ X-ray Photoelectron Spectroscopy Study of Lithium Interaction with Graphene and Nitrogen-Doped Graphene Films Produced by Chemical Vapor Deposition. *J. Phys. Chem. C* **2017**, *121*, 5108–5114. [[CrossRef](#)]
154. Kovtun, A.; Jones, D.; Dell'Elce, S.; Treossi, E.; Liscio, A.; Palermo, V. Accurate chemical analysis of oxygenated graphene-based materials using X-ray photoelectron spectroscopy. *Carbon* **2018**, *143*, 268–275. [[CrossRef](#)]
155. Yang, H.; Jiang, J.; Zhou, W.; Lai, L.; Xi, L.; Lam, Y.M.; Shen, Z.; Khezri, B.; Yu, T. Influences of graphene oxide support on the electrochemical performances of graphene oxide-MnO₂ nanocomposites. *Nanoscale Res. Lett.* **2011**, *6*, 531. [[CrossRef](#)] [[PubMed](#)]
156. Kumari, S.; Shekhar, A.; Pathak, D.D. Graphene oxide–TiO₂ composite: An efficient heterogeneous catalyst for the green synthesis of pyrazoles and pyridines. *New J. Chem.* **2016**, *40*, 5053–5060. [[CrossRef](#)]
157. Greczynski, G.; Hultman, L. A step-by-step guide to perform X-ray photoelectron spectroscopy. *J. Appl. Phys.* **2022**, *132*, 011101. [[CrossRef](#)]
158. Biesinger, M.C. Accessing the robustness of adventitious carbon for charge referencing (correction) purposes in XPS analysis: Insights from a multi-user facility data review. *Appl. Surf. Sci.* **2022**, *597*, 153681. [[CrossRef](#)]
159. van Attekum, P.M.T.M.; Wertheim, G.K. Excitonic Effects in Core-Hole Screening. *Phys. Rev. Lett.* **1979**, *43*, 1896–1898. [[CrossRef](#)]
160. Blyth, R.; Buqa, H.; Netzer, F.; Ramsey, M.; Besenhard, J.; Golob, P.; Winter, M. XPS studies of graphite electrode materials for lithium ion batteries. *Appl. Surf. Sci.* **2000**, *167*, 99–106. [[CrossRef](#)]
161. Proctor, A.; Sherwood, P. X-ray photoelectron spectroscopic studies of carbon fibre surfaces. I. carbon fibre spectra and the effects of heat treatment. *J. Electron Spectrosc. Relat. Phenom.* **1982**, *27*, 39–56. [[CrossRef](#)]
162. Xie, Y.; Sherwood, P. X-ray Photoelectron-Spectroscopic Studies of Carbon Fiber Surfaces. Part XII: The Effect of Microwave Plasma Treatment on Pitch-Based Carbon Fiber Surfaces. *Appl. Spectrosc.* **1990**, *44*, 797–803. [[CrossRef](#)]
163. Bourlier, Y.; Bouttemy, M.; Patard, O.; Gamarra, P.; Piotrowicz, S.; Vigneron, J.; Aubry, R.; Delage, S.; Etcheberry, A. Investigation of InAlN Layers Surface Reactivity after Thermal Annealings: A Complete XPS Study for HEMT. *ECS J. Solid State Sci. Technol.* **2018**, *7*, P329–P338. [[CrossRef](#)]
164. Sui, X.; Xu, R.; Liu, J.; Zhang, S.; Wu, Y.; Yang, J.; Hao, J. Tailoring the Tribocorrosion and Antifouling Performance of (Cr, Cu)-GLC Coatings for Marine Application. *ACS Appl. Mater. Interfaces* **2018**, *10*, 36531–36539. [[CrossRef](#)]
165. Zhao, D.; Sheng, G.; Chen, C.; Wang, X. Enhanced photocatalytic degradation of methylene blue under visible irradiation on graphene@TiO₂ dyade structure. *Appl. Catal. B Environ.* **2012**, *111–112*, 303–308. [[CrossRef](#)]
166. Ujjain, S.K.; Ahuja, P.; Sharma, R.K. Graphene nanoribbon wrapped cobalt manganite nanocubes for high performance all-solid-state flexible supercapacitors. *J. Mater. Chem. A* **2015**, *3*, 9925–9931. [[CrossRef](#)]
167. Rajender, G.; Kumar, J.; Giri, P. Interfacial charge transfer in oxygen deficient TiO₂-graphene quantum dot hybrid and its influence on the enhanced visible light photocatalysis. *Appl. Catal. B Environ.* **2018**, *224*, 960–972. [[CrossRef](#)]
168. Siburian, R.; Sihotang, H.; Raja, S.L.; Supeno, M.; Simanjuntak, C. New Route to Synthesize of Graphene Nano Sheets. *Orient. J. Chem.* **2018**, *34*, 182–187. [[CrossRef](#)]
169. Xing, M.; Li, X.; Zhang, J. Synergistic effect on the visible light activity of Ti³⁺ doped TiO₂ nanorods/boron doped graphene composite. *Sci. Rep.* **2014**, *4*, 5493. [[CrossRef](#)]
170. Ozkan, S.; Nguyen, N.T.; Mazare, A.; Cerri, I.; Schmuki, P. Controlled spacing of self-organized anodic TiO₂ nanotubes. *Electrochem. Commun.* **2016**, *69*, 76–79. [[CrossRef](#)]
171. Kusiak-Nejman, E.; Wanag, A.; Kowalczyk, Ł.; Kapica-Kozar, J.; Colbeau-Justin, C.; Medrano, M.G.M.; Morawski, A.W. Graphene oxide-TiO₂ and reduced graphene oxide-TiO₂ nanocomposites: Insight in charge-carrier lifetime measurements. *Catal. Today* **2017**, *287*, 189–195. [[CrossRef](#)]
172. Farooq, U.; Ahmed, F.; Pervez, S.A.; Rehman, S.; Pope, M.A.; Fichtner, M.; Roberts, E.P.L. A stable TiO₂-graphene nanocomposite anode with high rate capability for lithium-ion batteries. *RSC Adv.* **2020**, *10*, 29975–29982. [[CrossRef](#)]
173. Abdolkarimi-Mahabadi, M.; Bayat, A.; Mohammadi, A. Use of UV-Vis Spectrophotometry for Characterization of Carbon Nanostructures: A Review. *Theor. Exp. Chem.* **2021**, *57*, 191–198. [[CrossRef](#)]
174. Lai, Q.; Zhu, S.; Luo, X.; Zou, M.; Huang, S. Ultraviolet-visible spectroscopy of graphene oxides. *AIP Adv.* **2012**, *2*, 032146. [[CrossRef](#)]
175. Rong, X.; Qiu, F.; Zhang, C.; Fu, L.; Wang, Y.; Yang, D. Preparation, characterization and photocatalytic application of TiO₂-graphene photocatalyst under visible light irradiation. *Ceram. Int.* **2015**, *41*, 2502–2511. [[CrossRef](#)]

176. Emiru, T.F.; Ayele, D.W. Controlled synthesis, characterization and reduction of graphene oxide: A convenient method for large scale production. *Egypt. J. Basic Appl. Sci.* **2017**, *4*, 74–79. [[CrossRef](#)]
177. Zhang, Y.-P.; Xu, J.-J.; Sun, Z.-H.; Li, C.-Z.; Pan, C.-X. Preparation of graphene and TiO₂ layer by layer composite with highly photocatalytic efficiency. *Prog. Nat. Sci.* **2011**, *21*, 467–471. [[CrossRef](#)]
178. Luo, X.; Zhu, Z.; Tian, Y.; You, J.; Jiang, L. Titanium Dioxide Derived Materials with Superwettability. *Catalysts* **2021**, *11*, 425. [[CrossRef](#)]
179. Anucha, C.B.; Altin, I.; Bacaksiz, E.; Stathopoulos, V.N. Titanium dioxide (TiO₂)-based photocatalyst materials activity enhancement for contaminants of emerging concern (CECs) degradation: In the light of modification strategies. *Chem. Eng. J. Adv.* **2022**, *10*, 100262. [[CrossRef](#)]
180. Dong, H.; Zeng, G.; Tang, L.; Fan, C.; Zhang, C.; He, X.; He, Y. An overview on limitations of TiO₂-based particles for photocatalytic degradation of organic pollutants and the corresponding countermeasures. *Water Res.* **2015**, *79*, 128–146. [[CrossRef](#)]
181. Idris, N.H.M.; Cheong, K.Y.; Kennedy, B.J.; Ohno, T.; Lee, H.L. Buoyant titanium dioxide (TiO₂) as high performance photocatalyst and peroxide activator: A critical review on fabrication, mechanism and application. *J. Environ. Chem. Eng.* **2022**, *10*, 107549. [[CrossRef](#)]
182. Tu, W.; Zhou, Y.; Zou, Z. Versatile Graphene-Promoting Photocatalytic Performance of Semiconductors: Basic Principles, Synthesis, Solar Energy Conversion, and Environmental Applications. *Adv. Funct. Mater.* **2013**, *23*, 4996–5008. [[CrossRef](#)]
183. Luo, W.; Zafeiratos, S. A Brief Review of the Synthesis and Catalytic Applications of Graphene-Coated Oxides. *ChemCatChem* **2017**, *9*, 2432–2442. [[CrossRef](#)]
184. Velusamy, S.; Roy, A.; Sundaram, S.; Mallick, T.K. A Review on Heavy Metal Ions and Containing Dyes Removal Through Graphene Oxide-Based Adsorption Strategies for Textile Wastewater Treatment. *Chem. Rec.* **2021**, *21*, 1570–1610. [[CrossRef](#)]
185. Ajala, O.; Tijani, J.; Bankole, M.; Abdulkareem, A. A Critical Review on Graphene Oxide Nanostructured material: Properties, Synthesis, Characterization and Application in Water and Wastewater Treatment. *Environ. Nanotechnol. Monit. Manag.* **2022**, *18*, 100673. [[CrossRef](#)]
186. Quyen, T.T.B.; My, N.N.T.; Pham, D.T.; Thien, D.V.H. Synthesis of TiO₂ nanosheets/graphene quantum dots and its application for detection of hydrogen peroxide by photoluminescence spectroscopy. *Talanta Open* **2022**, *5*, 100103. [[CrossRef](#)]
187. Yu, X.; Lin, D.; Li, P.; Su, Z. Recent advances in the synthesis and energy applications of TiO₂-graphene nanohybrids. *Sol. Energy Mater. Sol. Cells* **2017**, *172*, 252–269. [[CrossRef](#)]
188. Faraldos, M.; Bahamonde, A. Environmental applications of titania-graphene photocatalysts. *Catal. Today* **2017**, *285*, 13–28. [[CrossRef](#)]
189. Stepić, K.; Ljupković, R.; Ickovski, J.; Zarubica, A. A short review of titania-graphene oxide based composites as a photocatalysts. *Adv. Technol.* **2021**, *10*, 51–60. [[CrossRef](#)]
190. Thakre, K.G.; Barai, D.P.; Bhanvase, B.A. A review of graphene-TiO₂ and graphene-ZnO nanocomposite photocatalysts for wastewater treatment. *Water Environ. Res.* **2021**, *93*, 2414–2460. [[CrossRef](#)] [[PubMed](#)]
191. Bilal, M.; Rizwan, K.; Rahdar, A.; Badran, M.F.; Iqbal, H.M. Graphene-based porous nanohybrid architectures for adsorptive and photocatalytic abatement of volatile organic compounds. *Environ. Pollut.* **2022**, *309*, 119805. [[CrossRef](#)] [[PubMed](#)]
192. Fathy, M.; Hassan, H.; Hafez, H.; Soliman, M.; Abulfotuh, F.; Kashyout, A.E.H.B. Simple and Fast Microwave-Assisted Synthesis Methods of Nanocrystalline TiO₂ and rGO Materials for Low-Cost Metal-Free DSSC Applications. *ACS Omega* **2022**, *7*, 16757–16765. [[CrossRef](#)] [[PubMed](#)]
193. Kausar, F.; Varghese, A.; Pinheiro, D.; Devi, S. Recent trends in photocatalytic water splitting using titania based ternary photocatalysts—A review. *Int. J. Hydrog. Energy* **2022**, *47*, 22371–22402. [[CrossRef](#)]
194. Ge, J.; Zhang, Y.; Heo, Y.-J.; Park, S.-J. Advanced Design and Synthesis of Composite Photocatalysts for the Remediation of Wastewater: A Review. *Catalysts* **2019**, *9*, 122. [[CrossRef](#)]
195. Giovannetti, R.; Rommozzi, E.; Zannotti, M.; D’Amato, C.A. Recent Advances in Graphene Based TiO₂ Nanocomposites (GTiO₂Ns) for Photocatalytic Degradation of Synthetic Dyes. *Catalysts* **2017**, *7*, 305. [[CrossRef](#)]
196. Zhao, X.; Zhang, G.; Zhang, Z. TiO₂-based catalysts for photocatalytic reduction of aqueous oxyanions: State-of-the-art and future prospects. *Environ. Int.* **2020**, *136*, 105453. [[CrossRef](#)] [[PubMed](#)]
197. Chen, D.; Cheng, Y.; Zhou, N.; Chen, P.; Wang, Y.; Li, K.; Huo, S.; Cheng, P.; Peng, P.; Zhang, R.; et al. Photocatalytic degradation of organic pollutants using TiO₂-based photocatalysts: A review. *J. Clean. Prod.* **2020**, *268*, 121725. [[CrossRef](#)]
198. Zhou, X.; Zhang, X.; Wang, Y.; Wu, Z. 2D Graphene-TiO₂ Composite and Its Photocatalytic Application in Water Pollutants. *Front. Energy Res.* **2021**, *8*, 612512. [[CrossRef](#)]
199. Jabbar, Z.H.; Ebrahim, S.E. Recent advances in nano-semiconductors photocatalysis for degrading organic contaminants and microbial disinfection in wastewater: A comprehensive review. *Environ. Nanotechnol. Monit. Manag.* **2022**, *17*, 100666. [[CrossRef](#)]
200. Padmanabhan, N.T.; Thomas, N.; Louis, J.; Mathew, D.T.; Ganguly, P.; John, H.; Pillai, S.C. Graphene coupled TiO₂ photocatalysts for environmental applications: A review. *Chemosphere* **2021**, *271*, 129506. [[CrossRef](#)]
201. Fu, P.; Feng, J.; Yang, H.; Yang, T. Degradation of sodium n-butyl xanthate by vacuum UV-ozone (VUV/O₃) in comparison with ozone and VUV photolysis. *Process Saf. Environ. Prot.* **2016**, *102*, 64–70. [[CrossRef](#)]
202. Faraz, M.; Shakir, M.; Khare, N. Highly sensitive and selective detection of picric acid using a one pot biomolecule inspired polyindole/CdS nanocomposite. *New J. Chem.* **2017**, *41*, 5784–5793. [[CrossRef](#)]

203. Atas, M.S.; Dursun, S.; Akyildiz, H.; Citir, M.; Yavuz, C.T.; Yavuz, M.S. Selective removal of cationic micro-pollutants using disulfide-linked network structures. *RSC Adv.* **2017**, *7*, 25969–25977. [[CrossRef](#)]
204. Preetha, S.; Ramamoorthy, S.; Pillai, R.; Narasimhamurthy, B.; Lekshmi, I. Synthesis of rGO-nanoTiO₂ composite mixture via ultrasonication assisted mechanical mixing method and their photocatalytic studies. *Mater. Today Proc.* **2022**, *62*, 5605–5612. [[CrossRef](#)]
205. Chen, X.; Jiang, X.; Huang, W. Evaluation and mechanism of ammonia nitrogen removal using sediments from a malodorous river. *R. Soc. Open Sci.* **2018**, *5*, 172257. [[CrossRef](#)]
206. Zhu, G.; Chen, J.; Zhang, S.; Zhao, Z.; Luo, H.; Hursthouse, A.S.; Wan, P.; Fan, G. High removal of nitrogen and phosphorus from black-odorous water using a novel aeration-adsorption system. *Environ. Chem. Lett.* **2022**, *20*, 2243–2251. [[CrossRef](#)]
207. Li, H.; Cao, Y.; Liu, P.; Li, Y.; Zhou, A.; Ye, F.; Xue, S.; Yue, X. Ammonia-nitrogen removal from water with gC₃N₄-rGO-TiO₂ Z-scheme system via photocatalytic nitrification-denitrification process. *Environ. Res.* **2021**, *205*, 112434. [[CrossRef](#)] [[PubMed](#)]
208. Yu, W.; Zheng, B.; Mao, K.; Jiang, J.; Luo, B.; Wu, X.; Tao, T.; Min, X.; Mi, R.; Huang, Z.; et al. Interfacial structure and photocatalytic degradation performance of graphene oxide bridged chitin-modified TiO₂/carbon fiber composites. *J. Clean. Prod.* **2022**, *361*, 132261. [[CrossRef](#)]
209. Yanwen, Z.; Feng, C.; Wei, L.; Jian, Q.; Liang, X.; Qianyu, L.; Yinlong, Z. Photocatalytic degradation of a typical macrolide antibiotic roxithromycin using polypropylene fibre sheet supported N-TiO₂/graphene oxide composite materials. *Environ. Technol.* **2022**. *online ahead of print.* [[CrossRef](#)] [[PubMed](#)]
210. Li, W.; Xu, X.; Lyu, B.; Tang, Y.; Zhang, Y.; Chen, F.; Korshin, G. Degradation of typical macrolide antibiotic roxithromycin by hydroxyl radical: Kinetics, products, and toxicity assessment. *Environ. Sci. Pollut. Res.* **2019**, *26*, 14570–14582. [[CrossRef](#)]
211. Meryem, S.S.; Nasreen, S.; Siddique, M.; Khan, R. An overview of the reaction conditions for an efficient photoconversion of CO₂. *Rev. Chem. Eng.* **2017**, *34*, 409–425. [[CrossRef](#)]
212. Chen, X.; Zhao, J.; Li, G.; Zhang, D.; Li, H. Recent advances in photocatalytic renewable energy production. *Energy Mater.* **2022**, *2*, 10. [[CrossRef](#)]
213. Som, I.; Roy, M. Recent development on titania-based nanomaterial for photocatalytic CO₂ reduction: A review. *J. Alloy. Compd.* **2022**, *918*, 165533. [[CrossRef](#)]
214. Domínguez-Espíndola, R.B.; Arias, D.M.; Rodríguez-González, C.; Sebastian, P. A critical review on advances in TiO₂-based photocatalytic systems for CO₂ reduction. *Appl. Therm. Eng.* **2022**, *216*, 119009. [[CrossRef](#)]
215. Kamal, K.M.; Narayan, R.; Chandran, N.; Popović, S.; Nazrulla, M.A.; Kovač, J.; Vrtovec, N.; Bele, M.; Hodnik, N.; Kržmanc, M.M.; et al. Synergistic enhancement of photocatalytic CO₂ reduction by plasmonic Au nanoparticles on TiO₂ decorated N-graphene heterostructure catalyst for high selectivity methane production. *Appl. Catal. B Environ.* **2022**, *307*, 121181. [[CrossRef](#)]
216. Ren, H.; Koshy, P.; Chen, W.-F.; Qi, S.; Sorrell, C.C. Photocatalytic materials and technologies for air purification. *J. Hazard. Mater.* **2017**, *325*, 340–366. [[CrossRef](#)]
217. Cao, J.-J.; Huang, Y.; Zhang, Q. Ambient Air Purification by Nanotechnologies: From Theory to Application. *Catalysts* **2021**, *11*, 1276. [[CrossRef](#)]
218. He, F.; Jeon, W.; Choi, W. Photocatalytic air purification mimicking the self-cleaning process of the atmosphere. *Nat. Commun.* **2021**, *12*, 2528. [[CrossRef](#)] [[PubMed](#)]
219. Tsang, C.H.A.; Li, K.; Zeng, Y.; Zhao, W.; Zhang, T.; Zhan, Y.; Xie, R.; Leung, D.Y.; Huang, H. Titanium oxide based photocatalytic materials development and their role in the air pollutants degradation: Overview and forecast. *Environ. Int.* **2019**, *125*, 200–228. [[CrossRef](#)]
220. Jiang, H.-Y.; Ouyang, Z.-Y.; Hu, R.; Wan, J.; Zhu, J.-J. Self-cleaning Finishing of Cotton Fabric with TiO₂/Ag₂S/rGO Composite. *Fibers Polym.* **2021**, *23*, 254–262. [[CrossRef](#)]
221. Hamidi, F.; Aslani, F. TiO₂-based Photocatalytic Cementitious Composites: Materials, Properties, Influential Parameters, and Assessment Techniques. *Nanomaterials* **2019**, *9*, 1444. [[CrossRef](#)]
222. Meda, U.S.; Vora, K.; Athreya, Y.; Mandi, U.A. Titanium dioxide based heterogeneous and heterojunction photocatalysts for pollution control applications in the construction industry. *Process Saf. Environ. Prot.* **2022**, *161*, 771–787. [[CrossRef](#)]
223. Demirel, C.S.U.; Birben, N.C.; Bekbolet, M. A comprehensive review on the use of second generation TiO₂ photocatalysts: Microorganism inactivation. *Chemosphere* **2018**, *211*, 420–448. [[CrossRef](#)]
224. Soleimani, M.; Ghasemi, J.B.; Ziarani, G.M.; Karimi-Maleh, H.; Badiei, A. Photocatalytic degradation of organic pollutants, viral and bacterial pathogens using titania nanoparticles. *Inorg. Chem. Commun.* **2021**, *130*, 108688. [[CrossRef](#)]
225. Padmanabhan, N.T.; Thomas, R.M.; John, H. Antibacterial self-cleaning binary and ternary hybrid photocatalysts of titanium dioxide with silver and graphene. *J. Environ. Chem. Eng.* **2022**, *10*, 107275. [[CrossRef](#)]
226. Sasidharan, S.; Nair, S.V.S.; Sudhakaran, A.; Sreenivasan, R. Insight into the Fabrication and Characterization of Novel Heterojunctions of Fe₂O₃ and V₂O₅ with TiO₂ and Graphene Oxide for Enhanced Photocatalytic Hydrogen Evolution: A Comparison Study. *Ind. Eng. Chem. Res.* **2022**, *61*, 2714–2733. [[CrossRef](#)]
227. Braiek, Z.; Ben Naceur, J.; Jrad, F.; Ben Assaker, I.; Chtourou, R. Novel synthesis of graphene oxide/In₂S₃/TiO₂ NRs heterojunction photoanode for enhanced photoelectrochemical (PEC) performance. *Int. J. Hydrog. Energy* **2021**, *47*, 3655–3666. [[CrossRef](#)]
228. Mehta, M.; Chandrabose, G.; Krishnamurthy, S.; Avasthi, D.K.; Chowdhury, S. Improved photoelectrochemical properties of TiO₂-graphene nanocomposites: Effect of defect induced visible light absorption and graphene conducting channel for carrier transport. *Appl. Surf. Sci. Adv.* **2022**, *11*, 100274. [[CrossRef](#)]

229. Ida, S.; Justin, S.S.; Wilson, P.; Neppolian, B. Facile synthesis of black N-TiO₂/N-RGO nanocomposite for hydrogen generation and electrochemical applications: New insights into the structure-performance relationship. *Appl. Surf. Sci. Adv.* **2022**, *9*, 100249. [[CrossRef](#)]
230. Esmaili, H.; Kowsari, E.; Ramakrishna, S.; Motamedisade, A.; Andersson, G. Sensitization of TiO₂ nanoarrays by a novel palladium decorated naphthalene diimide functionalized graphene nanoribbons for enhanced photoelectrochemical water splitting. *Mater. Today Chem.* **2022**, *24*, 100900. [[CrossRef](#)]
231. Gao, M.; Zhu, L.; Ong, W.L.; Wang, J.; Ho, G.W. Structural design of TiO₂-based photocatalyst for H₂ production and degradation applications. *Catal. Sci. Technol.* **2015**, *5*, 4703–4726. [[CrossRef](#)]
232. Wang, Q.; Yu, Z.; Liu, Y.; Zhu, X.; Long, R.; Li, X. Co-intercalation of TiO₂ and LDH to reduce graphene oxide photocatalytic composite membrane for purification of dye wastewater. *Appl. Clay Sci.* **2021**, *216*, 106359. [[CrossRef](#)]